Novel Nano-Engineered Titanium Surface for Direct Connective Tissue Attachment

Novel Nano-Engineered Titanium Surface for Direct Connective Tissue Attachment

A Thesis Presented by

Chia-Yu Chen

to

The Faculty of Medicine

In partial fulfillment of the requirements

For the degree of

Doctor of Dental Medicine

In the subject of

Oral Biology

Masazumi Nagai, DDS, PhD

Harvard School of Dental Medicine

Boston, Massachusetts

April, 2019

This thesis is dedicated to my family, Chien-Lung Chen and Chi-Chien Cheng, and my sister Fang-Yu Chen, for their love and unconditional support.

Table of Contents

Abstract

Novel Nano-Engineered Titanium Surface for Direct Connective Tissue Attachment

Introduction:

One of the greatest differences between natural teeth and dental implants lies in the attachment apparatus. Collagen fiber bundles connect the tooth to the gingiva in the form of connective tissue attachment which inserts perpendicularly to the root surface. On the contrary, bundles of connective tissue fibers run parallel to the implant surface at the transmucosal level which make for a vulnerable seal.

The goal of the present study is to develop a nano-engineered titanium surface with perpendicularly attached collagen that stimulate platelet activation for the restoration of periodontium-like connective tissue around dental implants.

Materials & Methods:

The titanium surface modification is executed in two stages. First, TiO_2 nanotube array is fabricated via anodization. Diameters and depths of TiO_2 nanotubes are controlled by applied voltage and duration. Subsequently, an electrophoretic fusion (EPF) method is applied to fuse type I collagen (Col-I) into nanotube arrays on the titanium surface. Surface morphology of the collagen-modified titanium surface was observed using

scanning electron microscopy (SEM), Fourier transform infrared spectroscopy (FTIR) and atomic force microscopy (AFM).

Next, platelet-rich plasma (PRP) is prepared and samples (tests and control) were incubated with PRP for 30 minutes, one hour and 3 hours on a see-saw table at 37 °C. At the end of the incubation period, the samples were rinsed and fixed for observation under SEM while supernatants were subjected to enzyme-linked immunosorbent assay (ELISA).

To verify the integration of fibroblast-produced Col-I to the nanoengineered surface, samples (tests and control) were co-cultured with fibroblasts using a cell culture insert with mesh size of 3 µm. At the end of the incubation period, samples were either dried in serial alcohol dehydration for SEM observation or stained with a FITC-conjugated anti-Col-I antibody for confocal fluorescence microscopy.

In another culture system, fibroblasts between passaged 10 ~20 were seeded directly onto sample (test and control) surfaces. 50 mg/mL of L-Ascorbic acid was supplemented every other day for 8 days. At the end of the incubation period, samples were fixed with 4% PFA for 20 minutes and store in phosphate buffered solution (PBS). The samples were subjected to observation with SEM, multiphoton laser scanning microscopy and RAMAN spectroscopy.

Results:

SEM with EDX observation revealed that a uniform array of nanotubes measuring 67 nm in diameter was obtained by anodization at 30 volts for 3 hours. Electrophoresis of type-I collagen through native PAGE gel into Ti nanotube surface resulted in Col-I depositions in a perpendicular fashion. SEM images showed a uniform array of perpendicular collagen fibrils deposited into and around the nanotubes while the presence of an amide C=O absorption peak at 1550 cm-1 in the spectrum was confirmed with FTIR. The perpendicularly attached Col-I to the nanotubes demonstrated a significantly more robust binding (compared to other methods of Col-I deposition), resistant to high-power sonication.

When platelet-rich plasma (PRP) was applied onto titanium, platelets aggregated on perpendicular collagen-fused nanotube surface while there were none or few for pure titanium surfaces at an early time point. Furthermore, confocal fluorescence microscopy revealed an increased amount of collagen on the modified Ti surfaces in a co-culture model with fibroblasts, confirming that fibroblast-derived Col-I fused with the engineered Col-I.

Polarized Raman spectroscopy revealed perpendicularly oriented collagen fibers extruding out from the nano-engineered collagen on nanotube-titanium surface.

Conclusions:

In this study, we hypothesized that our modified TiO_2 surface with perpendicular collagen-fused nanotube array would facilitate biomimetic restoration of peri-implant soft and hard tissue. The key innovation is the orientation of the fused Col-I. The nanotubes support the perpendicular insertion of Col-I monomers and these monomer projections, in terms, serve as the priming site for activation of in vivo healing process.

In this report, we have shown that the nano-engineered surface with perpendicular collagen coating promoted fibroblasts attachment and induced platelet activation. An i*n vitro* culture model revealed that fibroblasts secreted collagen fibrils attached to the engineered surface in a perpendicular fashion. We will move toward *in vitro* 3D culture model as well as *in vivo* mice animal model to further investigate the establishment of a direct connective tissue attachment to the modified titanium surface.

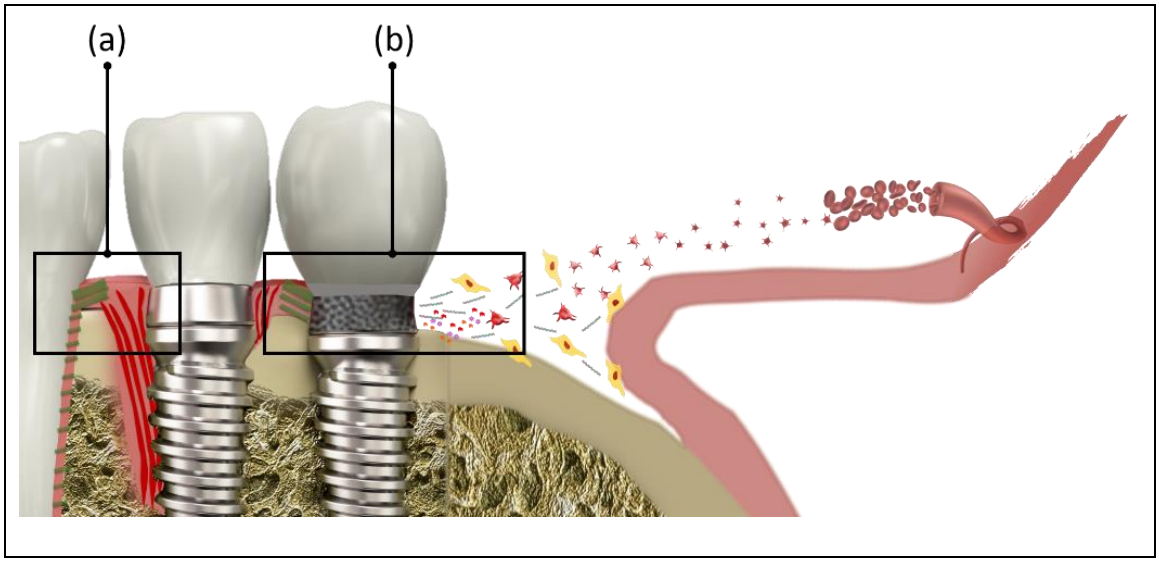

Fig 1. Schematic Summary of the Project

(a) Problem: Rapid bone loss due to weak soft tissue sealing of current abutment surface

(b) Solution: Novel engineered surface with perpendicular collagen triggers platelet wound repair, promotes strong epithelial sealing and provide priming sites for ligamental direct fiber insertions.

Chapter 1. Introduction

Since the introduction of the concept of “osseointegration” by Branemark et al, the use of endosseous dental implants for rehabilitation of missing teeth has become a routine treatment option.(1) Defined by Albrektsson et al, the term “osseointegration” refers to the direct contact between bone and implant at the light microscopic level; therefore, implants are essentially “ankylosed” to bone without a periodontal ligament.(2) Despite the high survival rate of dental implants, implant-related complications are being frequently reported and failures do occur. Growing numbers of implants are placed each year with frequent reports of implant-related complications. Among them, the prevalence of peri-implantitis is of great concern to all clinicians. Peri-implantitis is a pathological condition occurring in tissues around dental implants, characterized by inflammation in the peri-implant connective tissue and progressive loss of supporting bone.(3) According to a recent systematic review by Derks et al, the weighted mean prevalence of peri-implantitis is 22% (CI: 14-30%).(4) This is indeed a disappointing discovery for the patients and calls for a solution.

The etiology of peri-implantitis has yet to be fully elucidated but most agree that infection is a major attribute.(5) Many researchers, including Lindhe et al, have pointed out that bone loss is more rapid at the implant-bone interface for osseointegrated implants as compared with the tooth-bone interface.(6, 7) Comparing dental implants to

natural teeth, there lies significant differences in terms of the attachment apparatus.(8, 9) To minimize dental implant failures and complications, biosimilar integration of dental implants to the surrounding tissue especially at the transmucosal (gingiva) level is essential.(10)

The Nanoengineered titanium surface has been attracting more attention in recent years because nanoscale topography influences cell adhesion and osteoblast differentiation.(11) TiO_2 nanotubes created by electrochemical anodization, in particular, has become increasingly popular due to its simplicity and low cost.(12) Many investigators have demonstrated the potential of TiO_2 nanotubes to direct osteogenic differentiation of mesenchymal stem cells and promote osteoblast cell growth.(13)

The principal fibers of the periodontium are composed mainly of type I collagen (Col-I).(14) Collagen is synthesized by fibroblasts, chondroblasts, osteoblasts, odontoblasts and other cells.(14) An appealing feature of Col-I is the ability of Col-I monomers to self-assemble into fibrillar structures both in vivo and in vitro.(15) Its characteristic triple helix feature enables tunability in nanoengineering.(16) Furthermore, Col-I has an integrin $\alpha 2\beta 1$ binding domain and is also a well-known platelet activator.(17-20)

We hypothesized that through nanotube surface modification of the current machined titanium abutment surface and subsequent treatment with Col-I coating, the

biomimetic restoration of peri-implant soft tissue with direct connective tissue attachment can be achieved via endogenous signaling molecules released by activated platelets.

The aims of the study are

1) To fabricate and characterize the novel titanium surface that will facilitate a periodontium-like soft tissue healing

2) To evaluate the efficacy of platelet activation of the novel titanium surface

3) To validate the elongation of fibroblast-derive collagen from the engineered perpendicular collagen in the nanotube

Chapter 2. Review of Literature

I. Peri-implant vs. Periodontal Marginal Soft Tissues

The soft tissue structures enveloping a dental implant include the epithelial and connective tissue elements; in many ways, they are analogous to those surrounding the natural tooth. While the endosseous portion of a dental implant provides anchorage, the transmucosal portion facilitates attachment of the dental restoration and as in the case with teeth, this transmucosal layer must provide a physical and physiological barrier between the external oral environment and the underlying tissues.

Macroscopically, the periodontium and peri-implant soft tissues may appear similar, there are several fundamental differences in terms of their dimensions and mode of attachment. The biologic width, comprising of junctional epithelium (JE) attachment and connective tissue (CT) attachment is around 2.04 mm (0.97 mm for JE and 1.07 mm for CT) for natural teeth while the number increases to 2.5~4 mm (1.5-2 mm for JE and 1-2 mm for CT) for dental implants.(21, 22)

The junctional epithelium (JE), with its innermost cells forming the epithelial attachment apparatus, ensures a tight seal against the tooth surface. It plays a critical role in tissue homeostasis and is the first line of defense against microorganisms.(23) An Ultrastructural study revealed differences between JEs around natural teeth and dental implants. The periodontium of natural teeth is protected from bacterial invasion by the

firm sealing of the JE, attaching to the tooth surface via a basement membrane (BM).(24) However, this is not the case for dental implants; the peri-implant epithelium is clinically recognized to have poor attachment with few BM attachments.(25) It was shown that the baso-apical orientation was such that the BM faces the connective tissue side and apical cell membrane faces the implant side; in other words, JE around dental implants appeared to just "lean" on the implant surface.(26-28)

Previously, our research group has established an effective platelet-induced functional sealing with epithelial BM attachment to the titanium surface via a protease activated receptor 4- activating peptide (PAR4-AP) coating.(29) Through modification of titanium implant surface with PAR4-AP, we have shown that platelets aggregate on the modified surface and induce epithelial BM attachment to titanium surface. The established tight epithelial attachment completely blocked bacterial invasion.(30)

There is an even greater difference in terms of the connective tissue (CT) attachment between natural teeth and dental implants. Along the root surface, the tooth has groups of collagen bundles embedded into the cementum and protruding out in different directions. These principle collagen fiber bundles connect the tooth to the gingiva in the form of perpendicular/ direct CT attachment.(31) Functionally, the densely collagenous CT braces the marginal gingiva firmly against the tooth and provide the

rigidity to withstand masticatory forces without being deflected away from the tooth surface.(14)

Peri-implant CT attachment has somewhat similar clinical features to that of teeth; however, differences can be observed in the fiber orientation and cellular composition. Bundles of CT fibers run parallel to the implant surface.(32) Some have speculated that the inability to prevent apical migration of the junctional epithelium due to the parallel alignment of CT may be the reason for loss of crestal bone in an average of 1.5 to 2 mm, or “dieback” to the first thread commonly observed after one year in function.(33) Furthermore, it was found in an animal study that the CT close to the implant surface contained a large number of fibroblasts and these fibroblasts were oriented with their long axis parallel to the adjacent collagen fibers and to the implant surface.(34) Overall, the soft CT compartment of the peri-implant mucosa contained fewer fibroblasts, less vasculature and more collagen fibers when compared to that around teeth.(35, 36)

Most studies investigating the different surface characteristics on mucosal barrier formation did not observed differences among different implant systems.(37) Buser et al reported that surface characteristics (i.e. rough sandblasted, fine sandblasted and polished) did not influence the healing pattern of the peri-implant mucosal tissues.(35) In contrast, studies by Nevins et al suggested that it may be possible to

promote the formation of perpendicularly attached CT fibers to the implant surface.(9, 33) In these studies, a polarized light microscopy revealed functionally oriented collagen fibers attaching perpendicularly to precisely defined microchannels (8-12 μm in width and 6-12 μm in depth) created by laser ablation. It has been suggested that by altering the chemical characteristic of the implant surface rather than its topography, a perpendicular orientation of CT attachment can be achieved. A mixture of parallel and perpendicular CT orientation has been observed at chemically modified hydrophilic implant abutment.(38)

Although the CT attachment outcome with laser-microgrooved channels and hydrophilic surfaces are promising, both have few, if any, follow-up studies demonstrating the same perpendicular CT attachment and corresponding improved clinical outcomes. Further investigation is necessary to elucidate the effect of surface topography and chemistry on the establishment of peri-implant soft tissue attachment to mimic that of the natural teeth.

II. Nanoscale Surface Structure: TiO_2 Nanotubes

Nanoscale surface modifications of biomedical scaffolds have been shown to have important effects for cellular interactions. Abrams et al reported that an abundant collagen in the extracellular matrix connected the cells and that cells formed nanosized

fiber bundles with a regular structure of 66 nm.(39) With contact area between cells and substrates to be approximately 50 nm, surfaces with a nanoscale pattern can significantly improve cell adhesion.(40) There are myriads of methods to create nanoscale surface topography; in the case of titanium and its alloys, the more popular techniques are machining, blasting, sol-gel and anodization.(41-43)

Electrochemical anodization is a method that produces nanostructures on the surface of metal-based implants such as titanium (Ti), titanium-based alloys, Tantalum and Zirconium. The end results of the anodization process are the thickening of the oxide layer from the usual 5-10 nm oxide layer formed due to atmospheric oxidation. In an electrochemical cell, Ti or its alloy serves as the anode while another conducting metal, such as platinum (Pt) or copper (Cu), serves as the cathode. In most electrolytes, Ti releases electron and becomes positive ions that immediately interact with oxygen to form a compact TiO_2 layer. However, in the presence of fluoride containing electrolyte (eg. NH_4F and HF), fluoride species compete with oxygen to bind with titanium ions. The formed molecule, TiF_6 is soluble and thus pits began to form on the titanium surface. (Fig. 2) The concentration of fluoride, use of aqueous or non-aqueous solutions, voltage and duration of the current applied all influence the morphology tubular structures formed. Generally speaking, nanotubes produced in ethylene glycol (EtOH)-based non-aqueous solutions yield more regular and longer tubular structures over an extended

period of time.(44) Diameters of nanotubes increases with applied voltage while the length positively correlates with length of time the electric current is applied.(12, 45, 46)

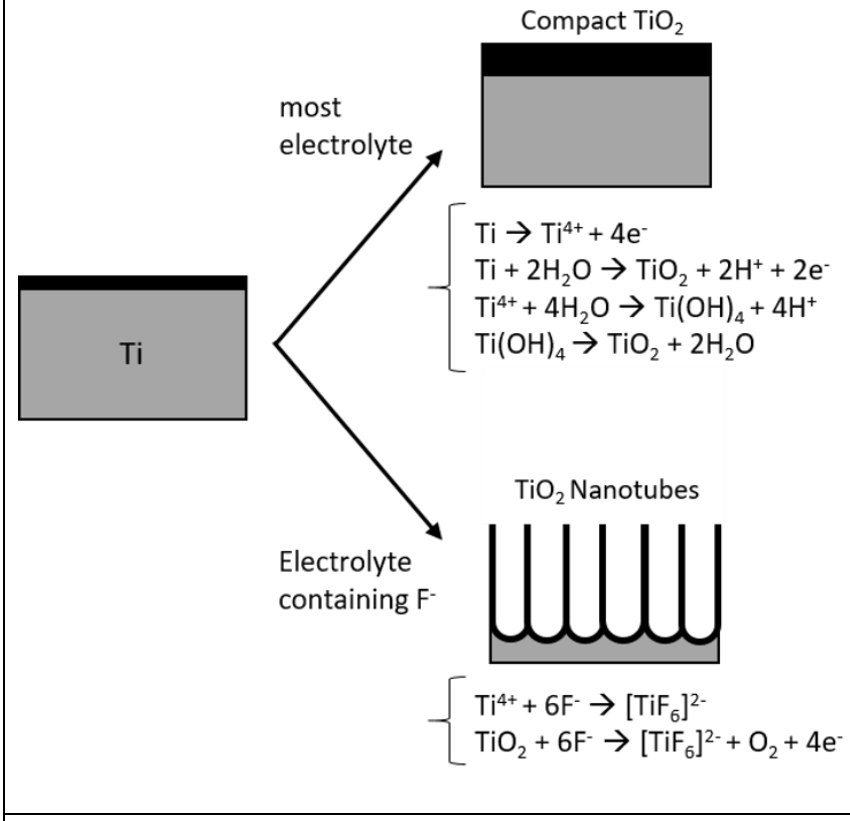

Fig 2. Electrochemical Anodization

III. Titanium Dioxide (TiO_2) Surface Coating: Electrophoretic Fusion (EPF) of Type I Collagen (Col-I)

Under atmospheric conditions, titanium becomes spontaneously coated by a 5 nm thick titanium dioxide layer (mostly TiO_2). Therefore, TiO_2, instead of titanium,

governs the interaction of titanium-based implants to the environment. There are three main crystalline phases of TiO_2: anatase, rutile and brookite. Anatase and rutile are the most studied and commercially utilized phases.(47)

Since roughness modification of the titanium surface alone does not change its inert nature, many researchers have been investigating further biomolecule functionalization of the implant surface. The popular molecules of choice are natural extracellular matrix proteins such as collagen, fibronectin, RGD type peptides and engineered protein fragments.(48) Collagen is a protein composed of different amino acids and it is responsible for the maintenance of the framework of tissue. Collagen fibrils have a transverse striation with a characteristic periodicity of 64 nm and this striation is caused by the overlapping arrangement of the tropocollagen molecules. The collagen molecule is a triple helical protein structure, consisting of three chains with a repenting sequence $(Gly\text{-}X\text{-}Y)_n$. A single type I collagen molecule is 1.5 nm in diameter and 300 nm in length. It bears a C-terminus comprising of a carboxyl end as well as a N-terminus comprising of an amine ends. The triple helix characteristic of Col-I enables tunability in nanoengineering.(49, 50)

The actual binding between the bioactive molecules to the titanium surface is the subject of much investigations. In the case of collagens, methods of immobilization include physical adsorption, wet deposition coating such as dip coating and layer-by-

layer (LBL), chemical bonding with EDC-cross-linking, electrospray deposition (ESD) and electrochemically assisted deposition method.(51) Electrophoretic deposition (EPD) is a traditional processing method in the ceramic industry that has been gaining interests for its potential in new material coating. EPD is a two-step process.(52-54) In the first step, charged particles move towards the oppositely charged electrode under the effect of externally applied electric field. In the second step, the particles deposit on the electrode. (Fig. 3) Advantages of the EPD method include a short operation time, cost-effectiveness, unneeded crosslinking agents and versatility for a arity of shapes and the ability to coat the inner surfaces of porous structures.

Considering parameters, such as particle size, viscosity, Zeta potential and etc., that influence the conventional EPD method as illustrated in Fig.3, we modified the technique and employed an semi-dry transblot system to achieve Col-I coating onto the titanium surface. We called our modified method “Electrophoretic fusion (EPF)”, which will be elaborated in a later chapter. We hypothesize that with Col-I, the triplicated anionic C-terminal ends will be attracted to the anode under electric current. When titanium is connected to the anode, Col-I monomers will be attracted towards the titanium surface to form a dentate chelate connection to the Ti surface.

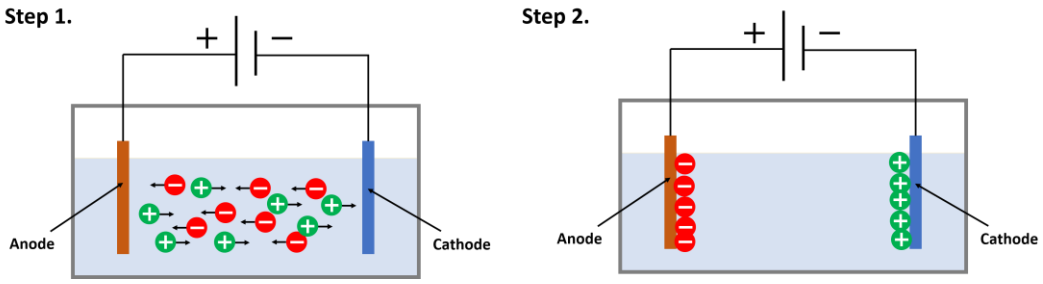

Fig 3. Conventional Electrophoretic Deposition (EPD)

IV. Wound Healing & Platelet-Rich Plasma (PRP)

Platelets plays a crucial role in wound healing by releasing a myriad of growth factors and cytokines.(55) Synthetic platelet derived growth factor (PDGF) is the current standard for biological growth factor use in tissue regeneration.(56) Its regenerative potential has been extensively proven in many in vitro, pre-clinical and clinical studies. (57) However, PDGF's high cost may diminish its potential clinical application worldwide. The use of autogenous platelet derivatives, especially platelet-rich plasma (PRP) is a popular alternative.

Platelet-rich plasma (PRP) is essentially an increased concentration of autologous platelets suspended in a small amount of plasma after centrifugation. The concentration of platelet often reaches 3-5 times compared to that of whole blood. Most PRP protocols call for the use of anticoagulant when collecting blood from patients. The collected blood undergoes two-step centrifugation at varying speeds. After the first spin

(often shorter in duration with approximately 1000g centrifugal force), blood separates into 3 layers: platelet poor plasma (PPP), buffy coat (containing leukocyte and platelet) and red blood cells. The top two layers containing plasma, leukocytes and platelets are collected into another tube without anticoagulant and undergo a second spin with longer duration. For the maximum strength in release of growth factors, the resultant PRP should be activated with bovine thrombin and CaCl prior to application.(58-60)

Platelet rich plasma (PRP) has been applied for periodontal regeneration due to its high concentration of platelets and growth factors expression. It has osteoinductive properties, it is easy to handle, available in large scale and has reduced risk of disease transmission or immunogenic reactions.(61) Among many growth factors present in PRP, fibroblast growth factor (FGF), platelet-derived growth factor (PDGF), vascular endothelial growth factor (VEGF), and transforming growth factor (TGF-B) exert great influence on tissue regeneration. PRP also enhances wound healing and facilitates cell proliferation, chemotaxis and differentiation.(62, 63)

Chapter 3. Surface Engineering and Characterization

I. Materials and Methods

A. Optimization of Titanium Oxide Nanotubes (TNTs) formation

For the present study, a smooth titanium plate (Ti) with 0.1 mm thickness (Grade-II titanium, GalliumSource, LLC, CA, US) was used. Anodization was applied to the titanium specimens. (Fig. 4) Copper was used as the cathode. Before anodization, titanium and copper samples were ultrasonically cleaned in 0.5% sodiumdodecyl sulfate (SDS; Sigma, MO, USA), deionized water, acetone (Sigma, MO, USA) and ethanol (Sigma, MO, USA), sequentially, for 20 minutes in each solvent, and then air-dried. The distance between the anodic titanium and cathodic copper was 2.5 cm. The anodization was performed in an electrolyte solution of ammonium fluoride (NH_4F) at 0.38 wt% and H2O at 1.79 wt% in ethylene glycol with constant voltages of 1, 5, 10, 20, 30 and 50 V for 1, 3 and 5 hours at each voltage. Specimens were washed in two-step sonication with 30% H_2O_2 for 2 minutes first, and then in 0.1 M acetic acid for 60 minutes. After cleaning, the specimens were air-dried and stored in a sealed container at room temperature until use.

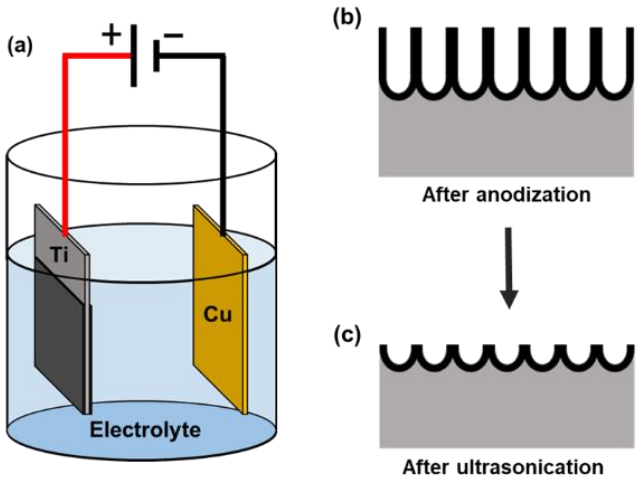

Fig 4. Schematic Representation of TiO_2 Nanotubes Fabrication
(a) Electrophoretic Cell Set-up: Titanium served as the anode while copper served as the cathode. There is a 2.5 mm distance between the electrodes
(b) Long tubular formation after anodization
(c) Removal for upper tubular layer through ultrasonication

B. Coating of Type-I Collagen (Col-I) to Titanium samples

To immobilize type I collagen (Col-I, Atelocollagen: Atelo Cell® IPC-30, KOKEN, Japan) onto the titanium surface, two methods were used: 1) the conventional chemical binding with an acid-based linker (CL) as a control and our new approach, and 2) electrophoretic fusion (EPF).

For the chemical binding method (CL), Col-I was linked to the titanium nanotube surface by means of phosphonic acid-based chemical linker with amide-end (10-CDPA; Dojindo Molecular Technology) as reported by Sugawara el al.(29) Briefly 1nM 10-CDPA

was chemically bound to TiO_2, and subsequently, Col-I was coupled to the amide-end by the EDC/NHS-chemistry.

EPF was carried out in a semi-dry transfer system. (Fig. 5) The transfer unit was assembled in the following order from the bottom: 1) anode of a semi dry blotter (Trans-Blot Turbo Transfer System®, BIO-RAD Laboratory, CA, USA); 2) 1x Tris glycine buffer (TGB)-wetted filter paper; 3) Titanium specimen: Smooth Ti (ST) and Nanotube Ti (NT); 4) 10% Native PAGE gel with 10% Col-I solution; 5) 1x TGB-wetted filter paper; and 6) cathode. The 10% native PAGE gel was casted according to manufacturer's directions (BIO-RAD Laboratory, CA, USA) with two major modifications. First, in order to fabricate native PAGE gel, SDS was not added into the mixture; this allowed for proteins to be run at a non-denaturing condition and moved depending on the protein's charge. Second, the Col-I solution (3 mg/mL) was mixed into the gel at a 1:10 ratio to achieve a final concentration of 0.3 mg/mL. The pH condition of the mixture was carefully maintained between 8-9 so that the amino acids along the collagen molecule were negatively charged. After the polymerization reaction was completed at room temperature for 20 minutes, the gel was stored at 4^0C overnight prior to use. Co-I was run at a constant voltage of 25 V for 2 minutes. After the transfer, the specimens were washed 3 times with PBS to remove unwanted residues.

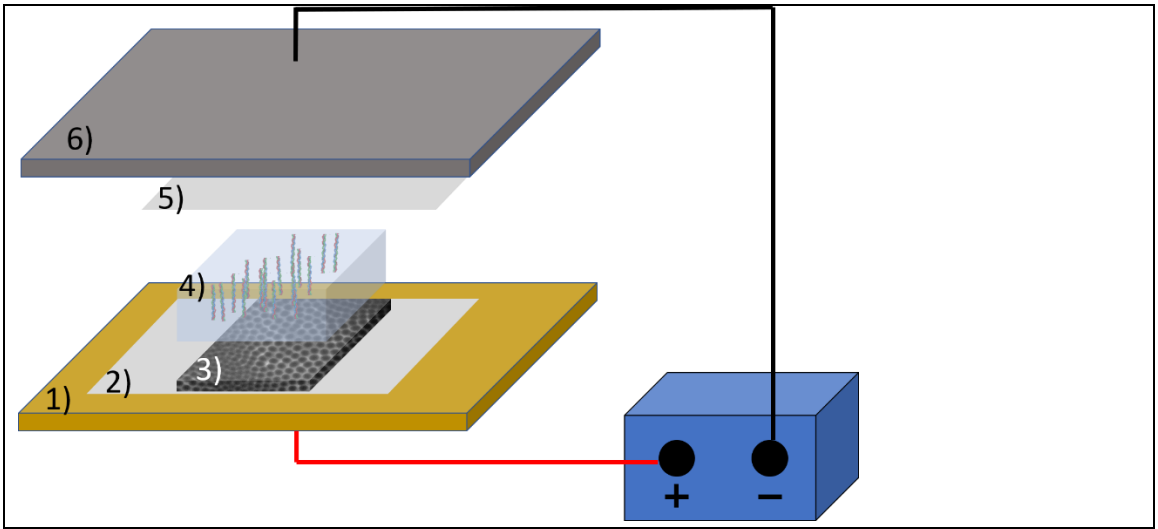

Fig 5. Schematic Representation of Col-I Electrophoretic Fusion (EPF)

C. Surface Characterization

The surface topography and molecular topology of titanium nanotube with/without Col-I coating was analyzed with scanning electron microscopy (SEM, Zeiss Supra 55VP field emission scanning electron microscope; ZEISS, Oberkochen, Germany) and an atomic force electron microscopy (Cypher AFM, Asylum Research, CA, USA) respectively. Briefly, the Co-I titanium was fixed in 4% paraformaldehyde (PFA), washed in water, and dehydrated in ethanol series to 100% (75%, 80%, 85%, 90%, 95% and 100%, 20 min in each incubation). Prior to SEM examination, the surface was sputtered coated with 5 nm of gold. The center of each titanium sample was cut into two 1.0 cm x 1.0 cm samples. Three regions of interest on the diagonal for each specimen were randomly selected. The number of clearly outlined nanotubes were counted using

Image J (National Institutes of Health, MD, USA). The nanotubes dimensions were also calculated. The average of triplet of each of 18 conditions were used for the data analysis.

The surface chemistry of the engineered surface was analyzed by Fourier Transform Infrared Spectroscopy Attenuated Total Reflection (FTIR-ATR) (Lumos FTIR Microscope, Bruker, MA, USA). The ATR crystal was a single bounce germanium crystal with 125 micron diameter. The treated titanium samples were examined using FTIR with 4 cm-1 resolution. Sixteen scans were averaged together for each data point over the range of 600-4000 cm-1. Following the FTIR peak assignments in the literature, the existence of Co-I on the titanium surface was determined by the backbone collagen amide I vibrations (C=O stretching vibration absorption peak: near 1651 cm-1) and amide II vibrations (N-H stretching vibration absorption peak: near 1519 cm-1) and hydrogen bond vibrations (Ti-OH absorption peak: 1089 cm-1). The data was processed by subtracting the FTIR spectra of the control titanium nanotube samples, from the test samples. The resulting difference spectra were baseline-corrected. The peak height of the absorbance peak corresponding to the amide I, amide II, and Ti-OH bonds of the FTIR-ATR spectrum was calculated using OPUS software.

The surface wettability was determined by contact angle measurement with a home-built system (Center for Nanoscale System at Harvard University, MA, USA). A

digital camera was used to capture an image of the 5 µl of droplet onto the different surfaces. Subsequently, an ImageJ plug-in was used to analyze the contact angle.

D. Binding Stabilities of Col-I to Titanium surfaces

The binding stabilitiy of CoI-I to different titanium surfaces was evaluated with a mechanical wash test. Tested specimens included the combination of two titanium surface topographies: 1) smooth titanium (ST) and 2) nanotube titanium (NT); and two Col-I binding methods: 1) CDPA-chemical linking (CL) and 2) electrophoretic fusion (EPF). In total, four types of specimens with different surface characteristics were examined and they were: 1) smooth titanium with chemical linking Col-I (ST-CL); 2) nanotube titanium with chemical linking Col-I (NT-CL); 3) smooth titanium with electrophoretic fusion of Col-I (ST-EPF) and 4) nanotube titanium with electrophoretic fusion of Col-I (NT-EPF). (Fig. 6) The specimens were sonicated in PBS with an ultrasonic disruptor (VWR Branson 250 Sonifier, MA, USA). The distance between the specimen and the ultrasonic probe tip was fixed at 10 cm. One cycle was 15 seconds at maximum power. The procedure was repeated for 3 and 10 cycles in each group with a 45 second pause between cycles. The presence of residual Col-I on the different surfaces after sonication was evaluated by Fourier Transform Infrared Spectroscopy

Attenuated Total Reflection (FTIR-ATR) (Lumos FTIR Microscope, Bruker, MA, USA).

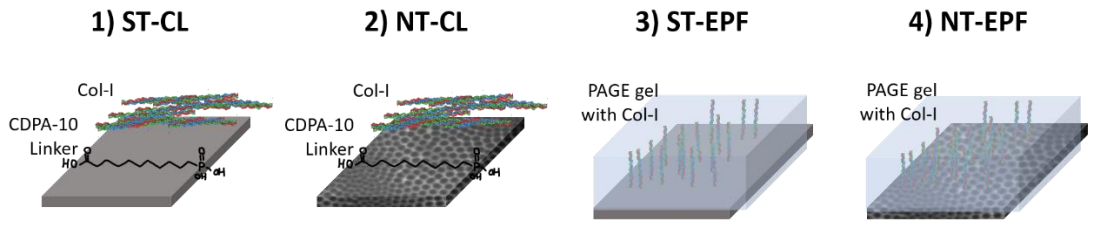

Fig 6. Schematic Representation of Specimen Groups

E. Statistical Analyses

Differences in the amount CoI-I on the tested titanium surfaces were compared using one-way analysis of variance (ANOVA) was conducted for intragroup and intergroup relationships. The average values of peak height in FTIR peaks of amide I, amide II, and Ti-OH bonds between groups were compared. The Tukey HSD post-hoc test was applied to assess differences that were statistically significant. The significance level adopted was 5% for all tests.

II. Results

Optimization of Titanium Nanotube Fabrication

Regularly aligned array of titanium nanotubes (TNTs) with an average diameter of 67 nm was observed in SEM when anodized at 30 V for 3 hours. (Fig. 7n) Under conditions with a lower voltage, nanotubes were not formed and yielded an irregular rough surface. (Fig. 7a~i) At 20 volts, regardless of duration, nanotubes were irregularly formed. (Fig. 7j~l) Extended anodization at 50 V for 5 hours yielded varied diameter TNTs ranging from 100 to 150 nm. (Fig. 5 p, q, r) Voltage and duration dependent TNT-diameter and number per field under SEM at x10,000 are shown in Table. 1. Based on the average diameter and the uniformity of TNT, we concluded that 30 V and 3 hours was the optimum combination of voltage and time.

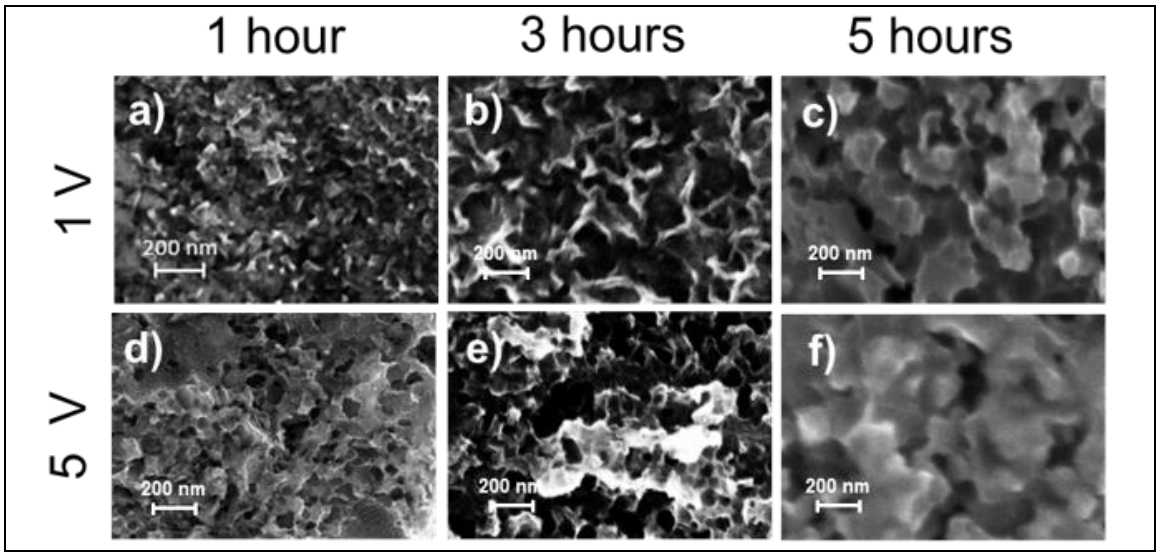

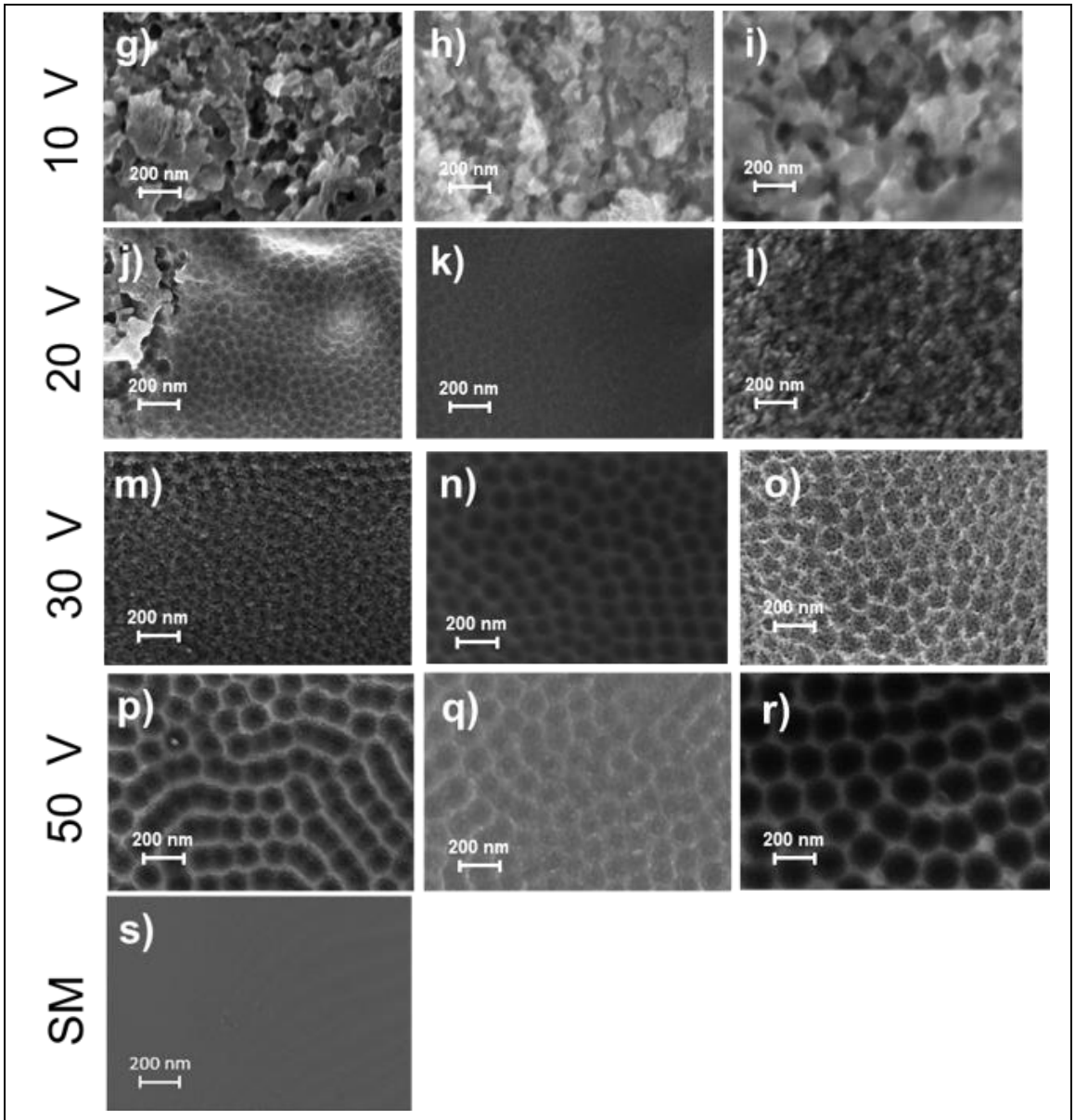

Fig 7. Nanotubes formed by anodization (Voltage v.s Time)

a) 1 V x 1 hour, b) 1 V x 3 hours, c) 1 V x 5 hours, d) 5 V x 1 hour, e) 5 V x 3 hours, f) 5 V x 5 hours, g) 10 V x 1 h, h) 10 V x 3 hours, i) 10 V x 5 hours, j) 20 V x 1 hour, k) 20 V x 3 hours, l) 20 V x 5 hours, m) 30 V x 1 hour, n) 30 V x 3 hours, o)30 V x 5 hours, p) 50 V x 1 hour, q) 50 V x 3 hours, r) 50 V x 5 hours, s) Smooth /control. Original magnification x 100000

Table 1. Measurement of nanotube number and diameter

Voltage (V)		0	1	5	10	20	30	50
Anodization (h)								
# of NTs observed	1h	NF	NF	NF	NF	IF	IF	457.8 ± 30.5
	3hs	NF	NF	NF	NF	IF	601.3 ± 13.2	331.6 ± 32.9
	5hs	NF	NF	NF	NF	IF	350.9 ± 26.0	311.1 ± 29.8
Diameter (nm)	1h	NF	NF	NF	NF	47.0 ± 3.7	66.4 ± 8.5	113.6 ± 8.6
	3hs	NF	NF	NF	NF	38.4 ± 3.0	67.0 ± 2.6	115 ± 5.3
	5hs	NF	NF	NF	NF	43.6 ± 3.0	68.3 ± 3.6	147.6 ± 11.7

# of TNT observed: View of magnification x 100000; NF=Not formed; IF: Irregular formation.

Type I Collagen Attachment

Representative SEM images of CoI-I attachment via EPF and CL onto smooth Ti (ST) and nanotube Ti (NT) surfaces are seen in Fig 8. The overhead view of TiO_2 surface in EPF groups showed CoI-I as nanodots indicating the perpendicular attachment on titanium surfaces. Nanodots of NT-EPF were aligned on the NT-edges and in the nanoholes (Fig. 8b) while poorly focused nanodots were seen on smooth Ti (Fig 8a). Diameter of each nanodot was between 5 nm and 10 nm suggesting perpendicular multimers of CoI-I. In CL groups, CoI-I was apparently laid down parallel to the long axis on both ST (Fig. 8c) or NT (Fig. 8d) surfaces.

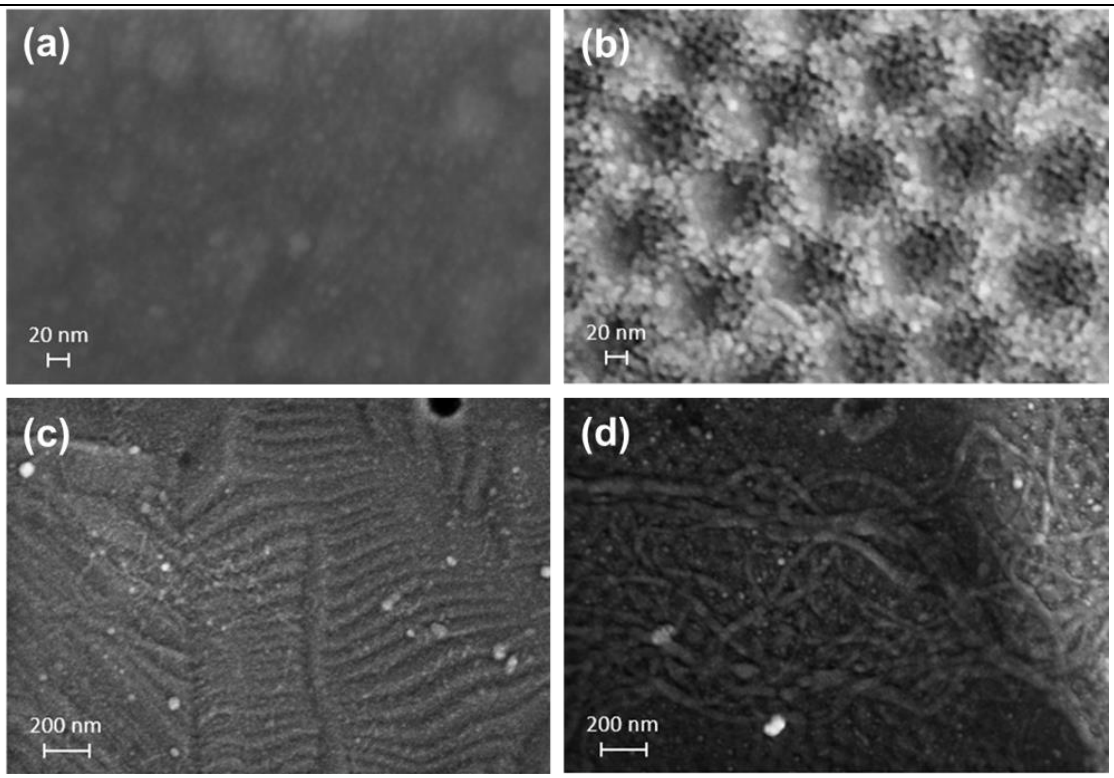

Fig 8. SEM images of Col-I attached to the titanium surfaces
a) ST-EPF, (b) NT-EPFI, (c) ST-CL and (d)NT-CL. (a), (b): Original magnification x 500000. (c), (d): Original magnification x 100000.

Different titanium surface topography and CoI-I attachment taken with AFM are shown in Fig. 9. While slight roughness was probed on ST (Fig. 9a1 and 9a2), a regularly aligned array of nanotubes was observed on the surface after anodization at 30 V for 3 hours (Fig. 9d1 and 9d2). On the ST-EPF surface, an amorphous nano-sized dot structure similar to the SEM image from Fig. 8a was observed (Fig. 9b2). On the NT-EPF surface, the collagen fibers protrude perpendicularly from the nanotube surface, following the contour of the nanotubes underneath (Fig. 9e1 and 9e2), and is remarkably different

from the AFM image of NT (Fig. 9d1, 9d2), indicating that collagen was inserted perpendicularly to the nanotube surface. In the CL groups, similar to SEM images (Fig. 8c, 8d), collagen was laid down parallel to the long axis on both ST and NT surfaces (Fig. 9c1, 9c2 and 9f1, 9f2).

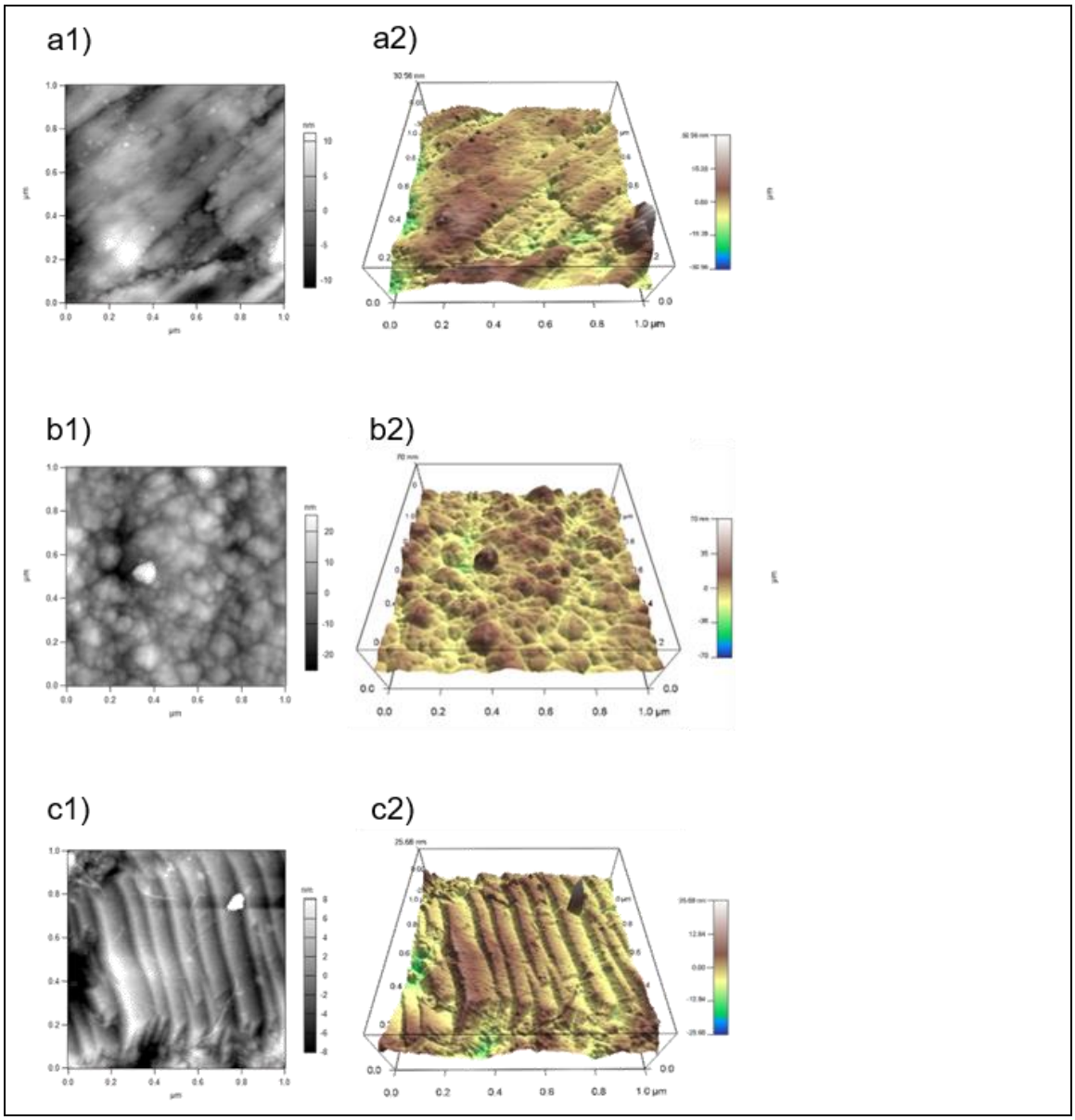

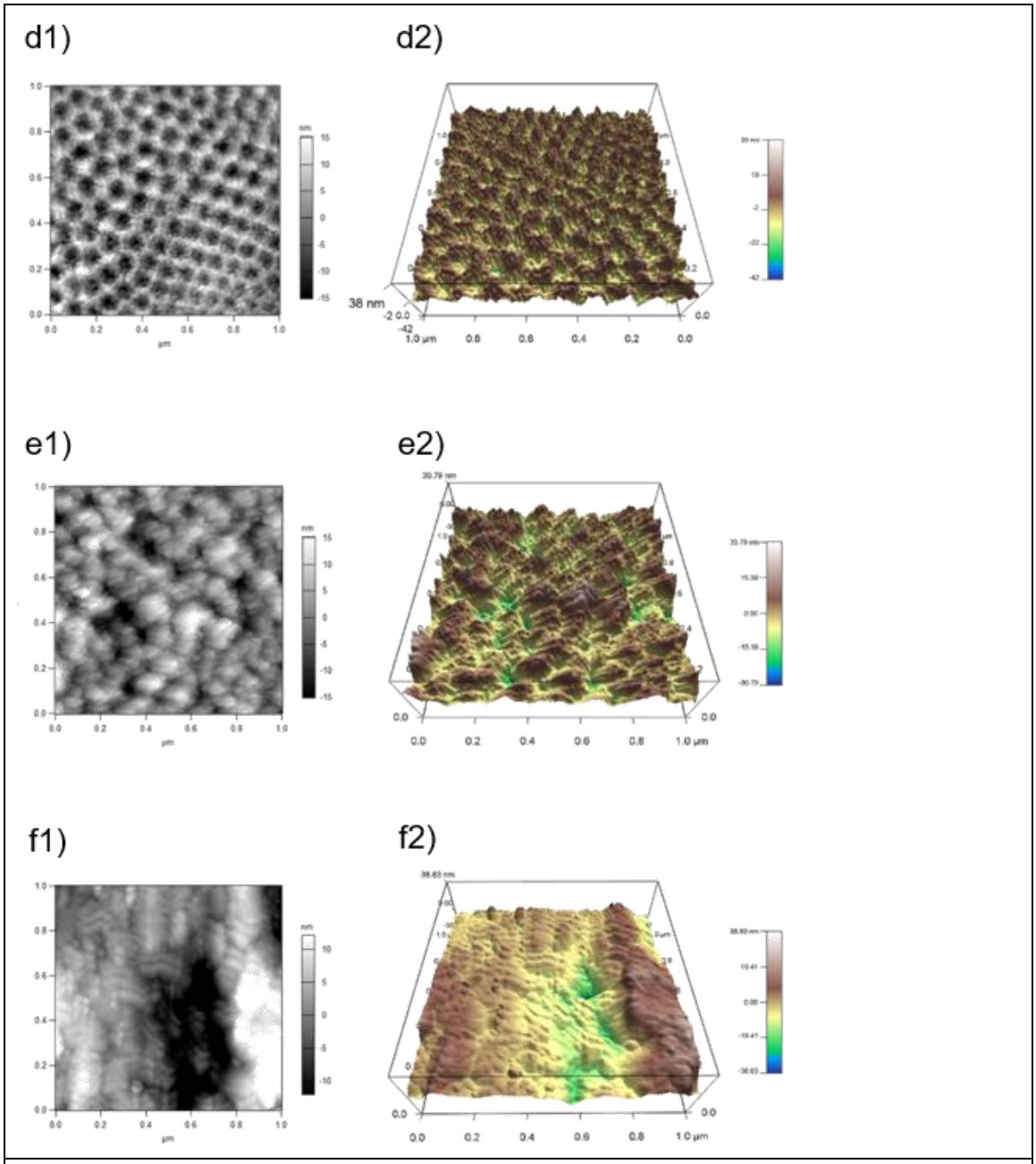

Fig 9. Surface topographic image through AFM

a1) ST, a2) 3D image of ST, b1) ST- EPF, b2) 3D image of ST-EPF, c1) ST-CL, c2) 3D image of ST-CL, d1) NT, d2) 3D image of NT, e1) NT-EPF, e2) 3D image of NT-EPF, f1)NT-CL, f2) 3D image of NT-CL.

Surface Wettability

Contact angle measurements were taken for the 6 different specimen surfaces (n=3). The mean contact angles were 75.92^0 for ST, 87.31^0 for NT, 73.15^0 for ST-CL, 69.28^0 for NT-CL, 55.60^0 for ST-EPF and 23.25^0 for NT-EPF. (Fig. 10-11) There is a statistically significant difference ($p<0.0001$, a 1-factor ANOVA and Tukey HSD post-hoc test) between NT-EPF and all other surfaces. This indicates that the NT-EPF surface has high surface energy and is highly hydrophilic.

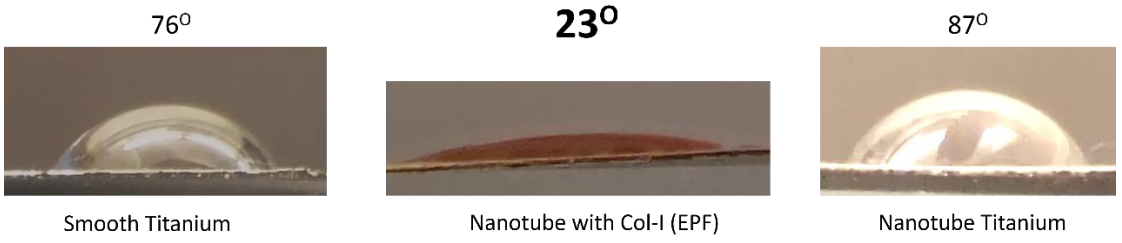

Fig 10. Representative Images of Water Contact Angle on Different Surfaces

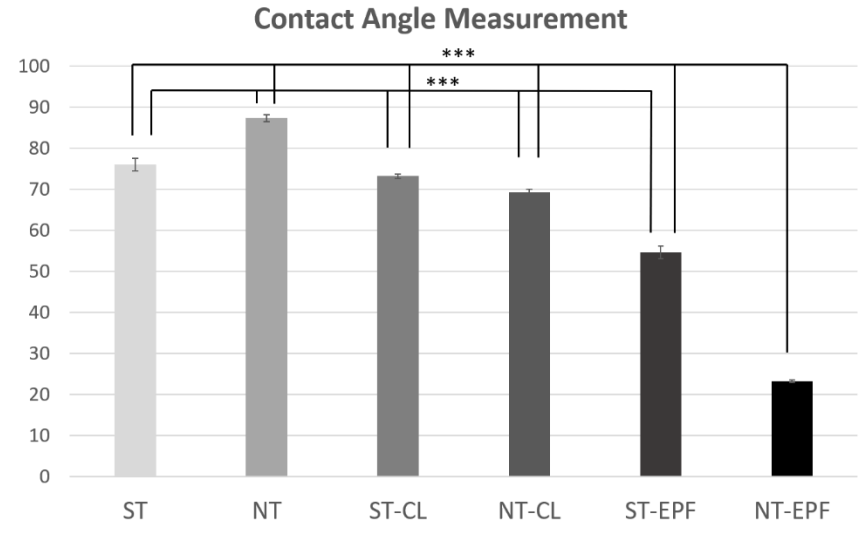

Fig 11. Average Contact Angle Measurements

Binding Stability of Col-I

CoI-I associated spectra were analyzed by FTIR-ATR to compare the binding stability on the titanium surfaces (Fig. 12). The Ti-OH absorption peak at 1089 cm^{-1} and the amide I bond at 1651 cm^{-1} were clearly identified after EPF on both ST and NT surfaces. After 3 sonication cycles, amide and Ti-OH bond peaks remained at 50% in NT-EPF and 10% in ST-EPF. The difference between the two groups was statistically significant (Fig. 13, $p<0.01$, 1-factor ANOVA and Tukey HSD post-hoc test). These peaks disappeared in CL groups (Fig. 12c) in the first 3 cycles of sonication. In NT-EPF, the bond peaks remained significant at higher than 10%. Similar trends in the reductions in the amide I and Ti-OH bonds were seen.

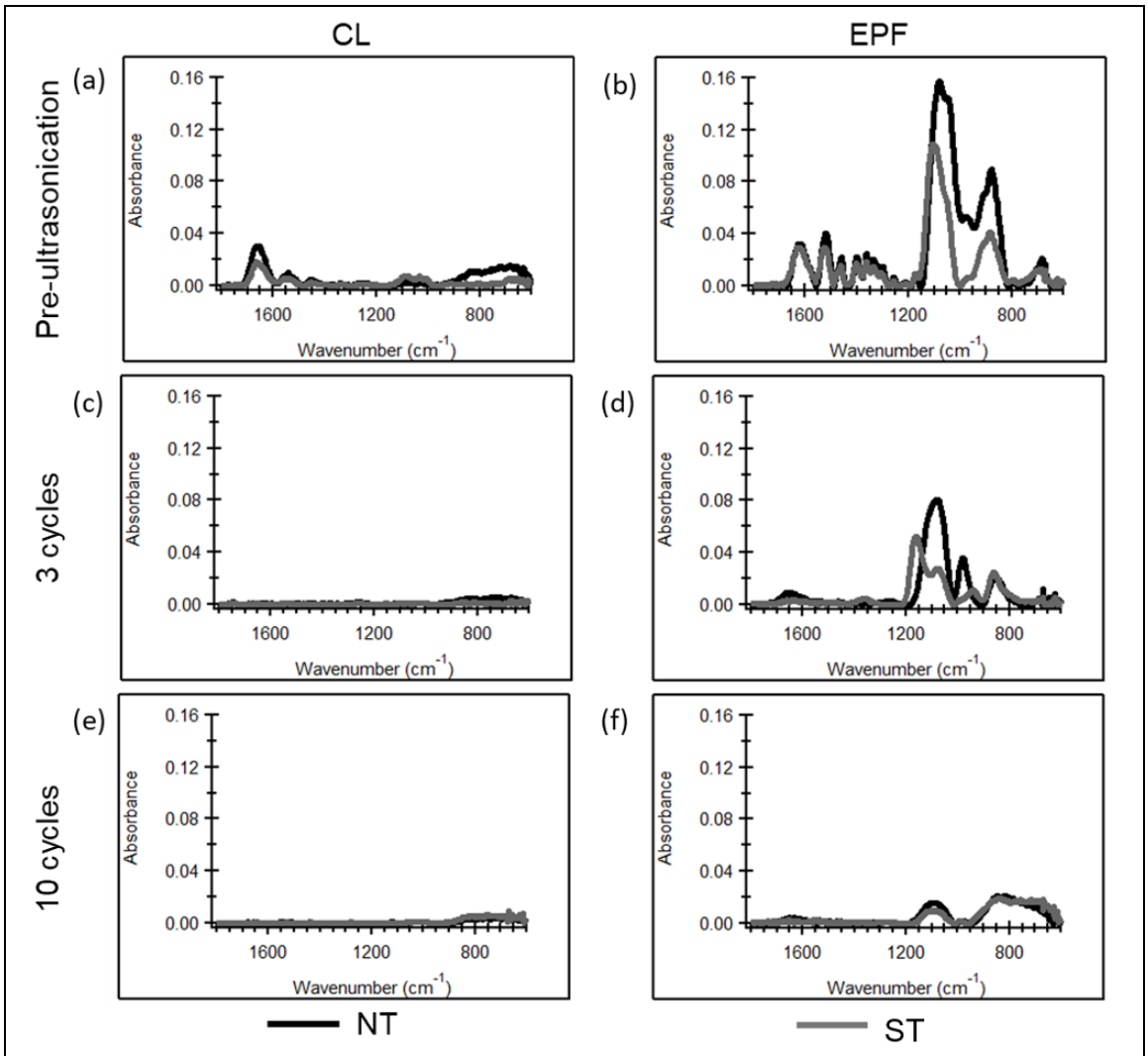

Fig 12. FTIR spectra of Col-I attached titanium surfaces with and without ultrasonication

(a) Pre wash of CL group, (b) Pre ultrasonication of EPF group, (c) 3 cycles of CL group, (d) 3 cycles of EPF group, (e) 10 cycles of CL group, (f) 10 cycles of EPF group

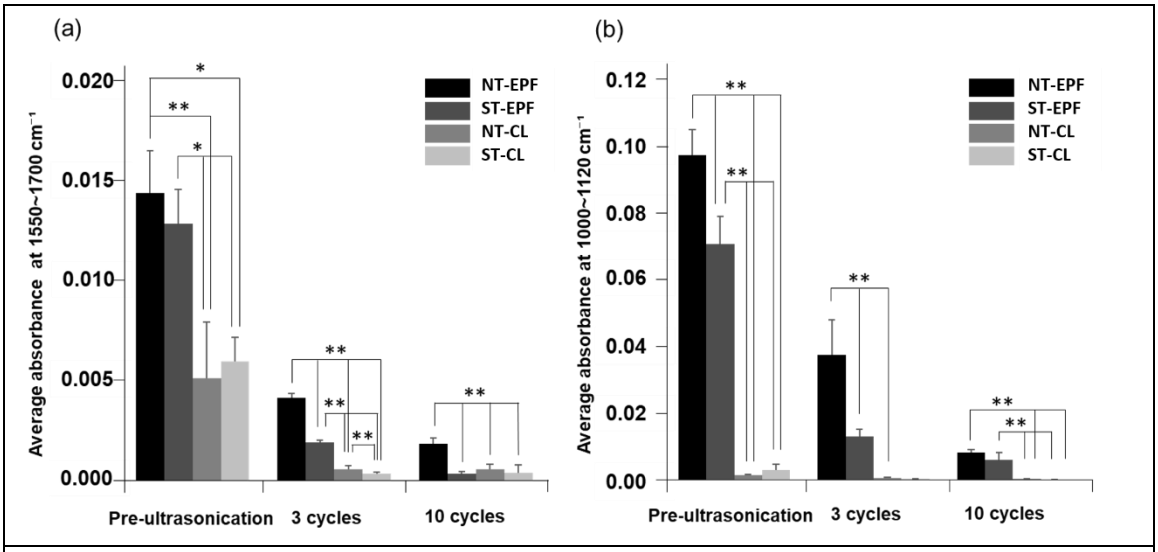

Fig 13. Average absorbance of the Amide bond and Ti-OH bond
a) Average absorbance at 1550~1700 cm^{-1} corresponding Amido bond, b) Average absorbance at 1000~1120 cm^{-1} corresponding Ti-OH bond. Error bars means represent means ± SD for n=3, *P<0.05, **P<0.01.

III. Discussion

In this study, we set out with the goal to fabricate a surface that would ultimately promote direct connective tissue attachment similar to that of a natural tooth. Type I collagen is the principal fiber of the periodontium and a major organic component in bone extracellular matrix. A single type I collagen molecule is 1.5 nm in diameter and 300 nm in length. As these molecules assemble into tertiary structures, the fibrillar collagens, their diameters increase to between 50 to 100 nm, with a specific pattern known as D-period. These fibers would go on to form fibers at the micron scale.(49) Since the fibrillar collagens are the building block to larger and more robust

collagenous tissue, we hypothesized that a titanium surface with nanotubes with a diameter ranging between 50~100 nm and a shallow depth of around 100 nm would serve as a good seeding vessel for collagen binding and supports the protrusion of 200 nm collagen molecules.

We experimented with different recipes of fluoride containing aqueous and/or non-aqueous electrolytes to fabricate titanium nanotubes (TNT) via anodization. We found that the most stable nanotube formation was achieved in an ethylene glycol based non-aqueous fluoride solution under 30 V for 3 hours. The resultant nanotube structure measured around 67 nm in diameter which was within the range we targeted. The nanotubular structures formed immediately following anodization are composed of amorphous phase TiO_2; therefore, an annealing treatment at high temperatures (400 to 600 ^{0}C) was often done by other research groups.(45) In our study, the initial formed nanotube layer after 3 hour-anodization was 2 μm in depth and the structure was brittle. Since our targeted nanotube depth was 100 nm, we did not perform the high temperature annealing; instead, we subjected the surface to a second step ultrasonication process in 30% H_2O_2 for 5 minutes to purposely remove the top layer of TNT, unveiling a glossy surface underneath with a uniform array of shallow nanotubes around 100 nm in depth.

We performed an elemental analysis using scanning electron microscopy with energy dispersive X-ray spectroscopy (SEM/EDX) before and after anodization to examine possible chemical residues that could affect Col-I bonding. We found an elevated level of fluoride despite an extended one-hour ultrasonic bath in distilled water after H_2O_2 treatment. (Fig. 14a) We then used 0.1 M acetic acid solution to thoroughly wash the surface. Our results indicated that we have greatly reduced the fluoride content. (Fig. 14b)

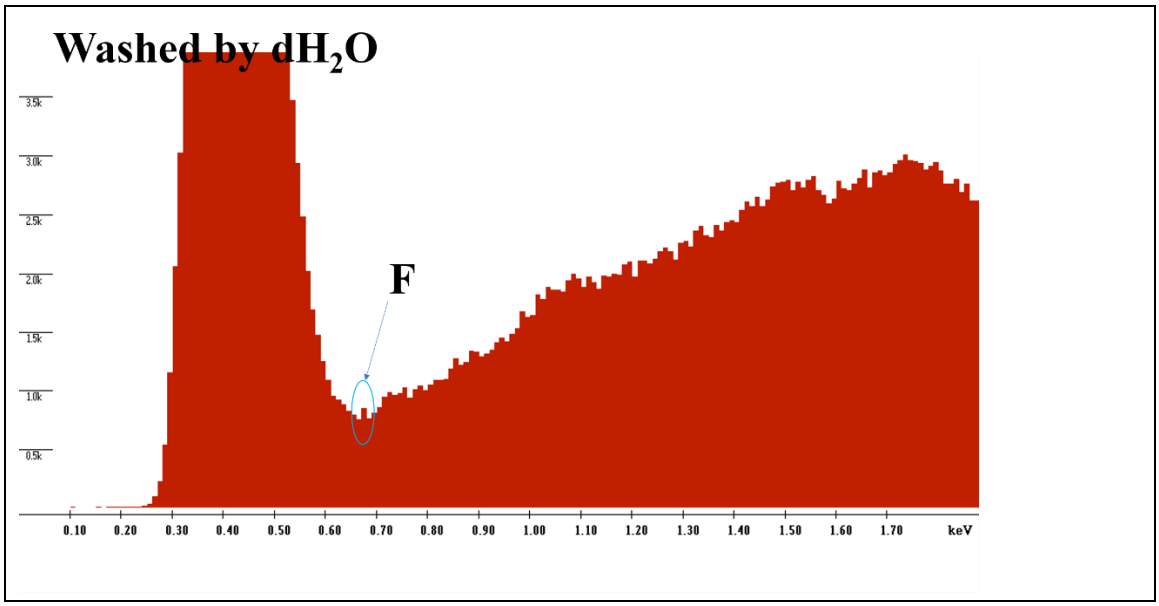

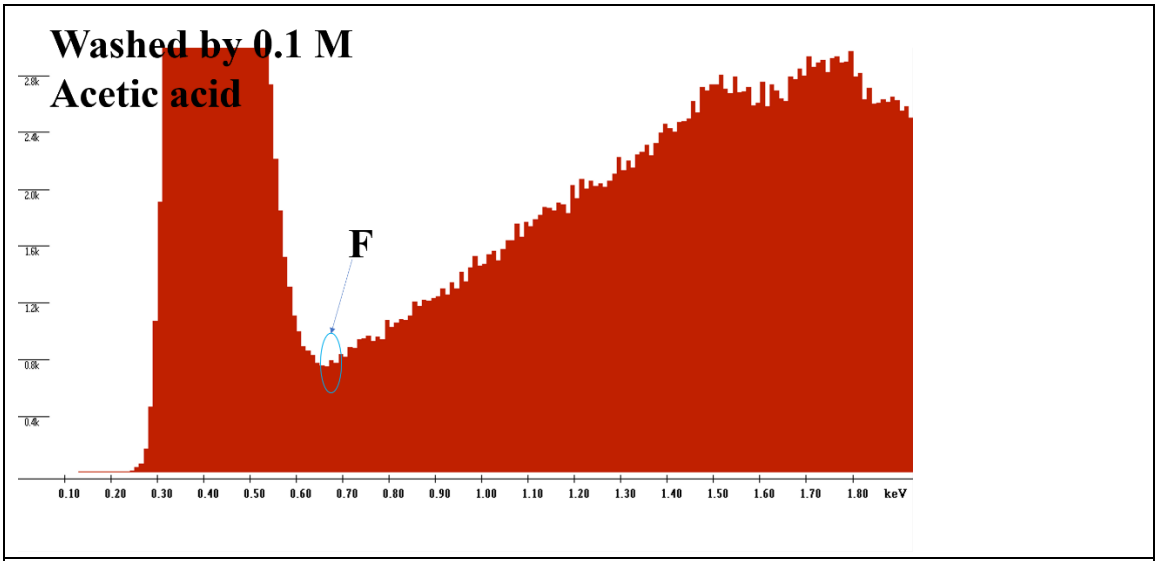

Fig 14. EDX Surface Elemental Analysis after Different Post-anodization Washing

Several technologies have been explored to alter the titanium surface with bioactive molecules. Biomolecules have been directly immobilized on titanium by passive adsorption or by covalent immobilization via a chemical linker. The major benefit of the conventional electrophoretic deposition (EPD) process is that it obviates the use of a chemical linker which is often harmful to cells; however, the efficacy of EPD is affected greatly by the size of the molecule. The novelty and key success of our modified electrophoretic fusion (EPF) lies in the use of a native polyacrylamide gel (PAGE) which would allow for an orientation-defined Col-I fusion. Triplet C-termini of Col-I are negatively charged under the pH of the native PAGE system; thus, the triplet negative C-termini are beaconed towards anodic TNT through the gel mesh to react with hydroxyl group on the titanium surface. As shown in the SEM and AFM images, the NT-

EPF surface had well-defined peaks and valleys of Col-I array. As revealed by FTIR, the presence of a Ti-OH absorption peak at 1089 cm^{-1} found only on EPF surfaces confirmed the direct Col-I binding to titanium. Tripe carboxylic acid residues have two potential binding modes, monodentate and bidentate to TiO_2.(64) In addition to the C-term dentate bindings, acidic groups in the collagen chains also form dentate bond to the side wall of the TNT, yielding the stable binding we termed EPF.

In anticipation of the application of our modified surface to the abutment level of a dental implant, we must bear in mind that clinically, dentists and or dental hygienists often use an ultrasonic instrument with a maximum power of 25 to 40 kHz/40 to 45 W for dental scaling; therefore, the Col-I binding must be able to withstand this force. We used an ultrasonic disrupter with a frequency of power of 20kHz/250 W, which is 5 times stronger than that used in the clinic to examine the Col-I binding. Our results indicated that the NT-EPF surface was able to withstand the strong ultrasonic disruption possibly due to the robust Col-I dentate fusion to TiO_2 by EPF method and the more surface area for attachment offered by the nanotube topography.

A major pitfall in our study was the use of grade 2 titanium, instead of Ti6Al4V, which is the primary alloy used in the orthopedic industry as well as in dentistry. We expect that our two-step surface fabrication process will work on other titanium alloys.

We have shown successful formation of an organized array of nanotubes on a commercially available titanium retention pin (Ti6Al4V, Nordin, Switzerland). (Fig. 15)

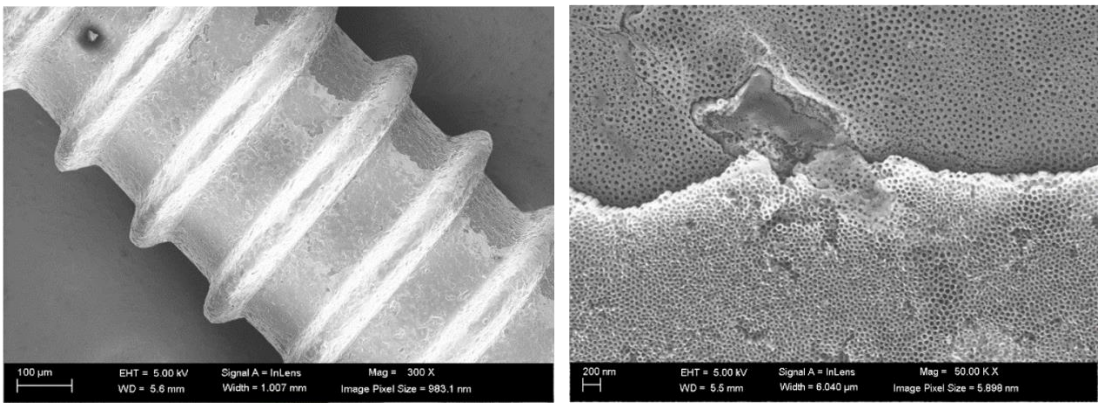

Fig 15. Nanotube Formation on a Commercially Available Titanium Retention Pin

Chapter 4. Cellular Response and Platelet Activation

I. Materials and Methods

A. Titanium Surface Fabrication

Five types of titanium surfaces were fabricated for the following experiments. For nanotube topography, the optimized setting as determined in the previous chapter was used. The five types of surfaces are: 1) smooth Ti (ST); 2) nanotube Ti (NT); 3) smooth Ti with chemical linking Col-I (ST-CL); 4) nanotube Ti with chemical linking Col-I (NT-CL) and 5) nanotube Ti with electrophoretic fusion of Col-I (NT-EPF).

B. Cell Culture and Maintenance of Human Keratinocyte Cell Line (OBA9) and Mouse Fibroblast Cell Line (NIH3T3)

Human gingival epithelial cell line OBA9 cells (Professor Murakami at Osaka University, Japan) were maintained in keratinocyte-SFM medium (Thermo Fisher Scientific) at 37°C in 5% CO_2 and 95% atmospheric air. Mouse fibroblasts NIH3T3 cells were maintained in DMEM medium (Thermo Fisher Scientific) supplemented with 10% FBS at 37°C in 5% CO_2 and 95% atmospheric air. For both types of cell lines, cells between 4~10 passages were used in the following experiments.

C. Cell Attachment to Titanium Surface

Attachment of epithelial cells and fibroblasts to the modified TiO_2 surface was evaluated as attached number and mode using a cell counting kit (CCK8, Dojindo molecular technology, WA, USA) and scanning electron microscopy (Zeiss Supra 55VP; Zeiss), respectively. Cells were seeded on 5 types of surfaces at 100k cells/cm^2 in 200 µL of culture medium in each well of 48 well plate and settled in the culture for 3 hours. Unbound cells were then gently washed off with the culture medium and the remaining cells were further cultured in 200 µl of culture medium supplemented with CCK8 reagent for another 3 hours. One hundred µL of CCK8 reaction was transferred to a 96-well plate for OD reading. Cells on each sample surface were washed with PBS and fixed in 4% PFA for SEM analysis. (Zeiss Supra 55VP; Zeiss).

In another experiment, the attachment of fibroblasts to the titanium surface over an extended incubation period was investigated as attached number of viable cells and mode. Cell viability was evaluated with a cell luminescent viability kit (CellTiter-Glo®, Promega, WI, USA). Cells were seeded on the same 5 types of surfaces at 100k cells/cm^2 in 200 µL of culture medium in each well of 48 well plate and settled in the culture for 24, 48 and 72 hours. Unbound cells were then gently washed off with the culture medium and specimens were transferred to a new well where a 200 µl mixture of culture medium and CellTiterGlo solution at 1:1 ratio was added. Cell lysis was induced by 2-minute vigorous shaking with an orbital shaker and the plate was left to

stabilize for 10 minutes before luminescent reading. Cells on each sample surface were washed with PBS and fixed in 4% PFA for SEM analysis (Zeiss Supra 55VP; Zeiss).

D. Platelet-Rich Plasma (PRP) Preparation

Fresh human whole blood collected with 10% ACD and shipped under ambient temperature was purchased from BioIVT (ELEVATING SCIENCE®, USA). Platelet-rich plasma (PRP) was prepared according to a previously published protocol.(65) Tubes containing whole blood were centrifuged at 3600 rpm with a centrifuge machine (Salvin Dental, NC, USA) with a 7.5 cm radius, equivalent to 1000g for 2 minutes and 15 seconds. After the whole blood separates into two layers, the upper light-yellow plasma layer was transferred into a new tube, not containing anti-coagulant. The new tubes, now containing only the plasma layer, were centrifuged at the same setting for another 5 minutes. The plasma was separated into an upper platelet-poor plasma (PPP) layer and a red pellet consisted of concentrated platelets at the bottom. For every 10 mL of final activated PRP, six tubes of whole blood (10 cc each) were used. The pellets generated from each tube were resuspended with 6 mL of PPP to produce inactivated PRP. Prior to use, 4 mL of PBS containing 143 mg of $CaCl_2$ was added to produce 10 mL of activated PRP.

E. Titanium Samples and PRP Incubation

Titanium specimens with the same 5 types of surfaces were placed at the bottom of a 24-well plate (n=4 for each group). Activated PRP (1 mL per well) was inoculated onto the samples. The plate was placed on a rocking table at 37^0C for different time points (30 minutes, one hour and three hours). At each time point, plasma was collected and stored at 4^0C until assay. A part of the 3-hour samples (n =3 for each group) were washed with PBS and placed into a new 24-well for overnight incubation in DMEM medium and the medium was collected the next day. For the collected plasma and medium, levels of platelet-related growth factors and cytokines such as platelet derived growth factor-AB (PDGF-AB), transforming growth factor-β (TGF-β), vascular endothelial growth factor (VEGF) and tumor necrosis factor-α (TNF-α) were evaluated with sandwiched enzyme-linked immunosorbent assay (ELISA) kits (R&D Systems, MN, USA). The remaining samples were fixed for SEM observation (Zeiss Supra 55VP; Zeiss).

F. Down Culture Model for Cell Migration to PRP-conditioned Titanium Surface

To evaluate the effect of the combination of different surface characteristics and platelet-related factors to fibroblasts, a down culture model was employed. (Fig. 16) In a 48-well cell culture-treated plate, fibroblasts were seeded at 100k cells/cm^2 in 400 µL of culture medium and settled overnight in the incubator. The next day, titanium specimens with the same 5 types of surfaces (n=4 per each surface type) were

incubated with activated PRP for 3 hours as described previously. At the end of the incubation, the samples were washed with PBS and transferred into the 48-well plate now containing overnight culture of fibroblasts. The specimens were placed with the treated surface facing down to the bottom of the well. At 48 and 72 hrs, the specimens were gently rinsed to remove unbound cells and processed for evaluations with a cell luminescent viability kit (CellTiter-Glo®, Promega, WI, USA) and SEM (Zeiss Supra 55VP; Zeiss).

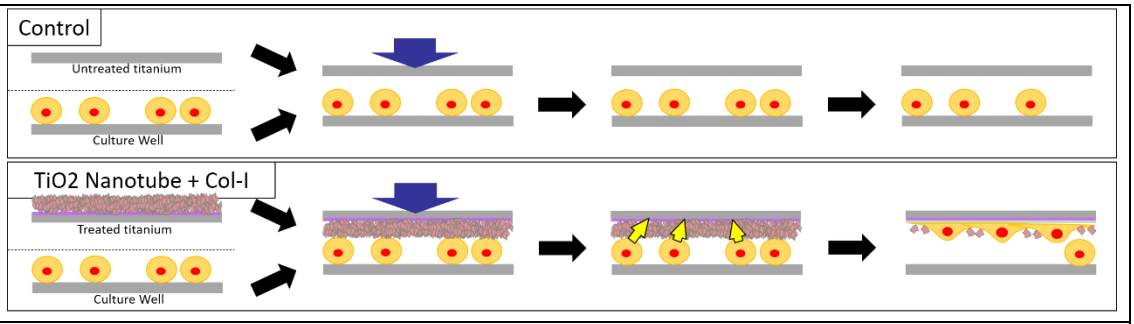

Fig 16. Schematic Representation of the Down Culture Model

G. Statistical Analyses

To compare the significant differences in the number of cells attached to the specimen surfaces as well as ELISA cytokines concentration, one-way analysis of variance (ANOVA) was conducted. The Tukey HSD post-hoc test was applied to assess differences that were statistically significant. The significance level adopted was 5% for all tests.

II. Results

Epithelial Attachment

The mode of epithelial attachment on each treated titanium surface was identified by SEM ultrastructure (Fig. 17). On ST and NT surfaces without CoI-I, limited numbers of epithelial cells were seen (F17a1, b1). In addition, these cells exhibited round-up morphology of weak adhesion (F17a2, b2). On the other hand, on ST and NT surfaces with CL-mediated parallel CoI-I coating, cells with widely spread plasma membrane occupied the surface (F17c1, 2, d1, 2). On the NT-EPF with perpendicular nanodot CoI-I surface, round up epithelial cells were sparsely seen (F17e1, 2). In addition, NT-EPF showed limited numbers of epithelial cells in the comparison to relative cell amount on other group surfaces measured by CCK8 reagent (Fig. 18).

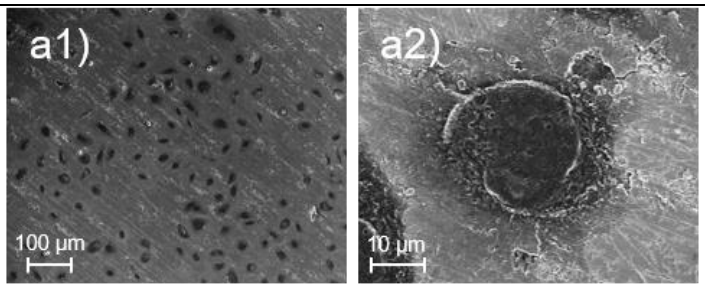

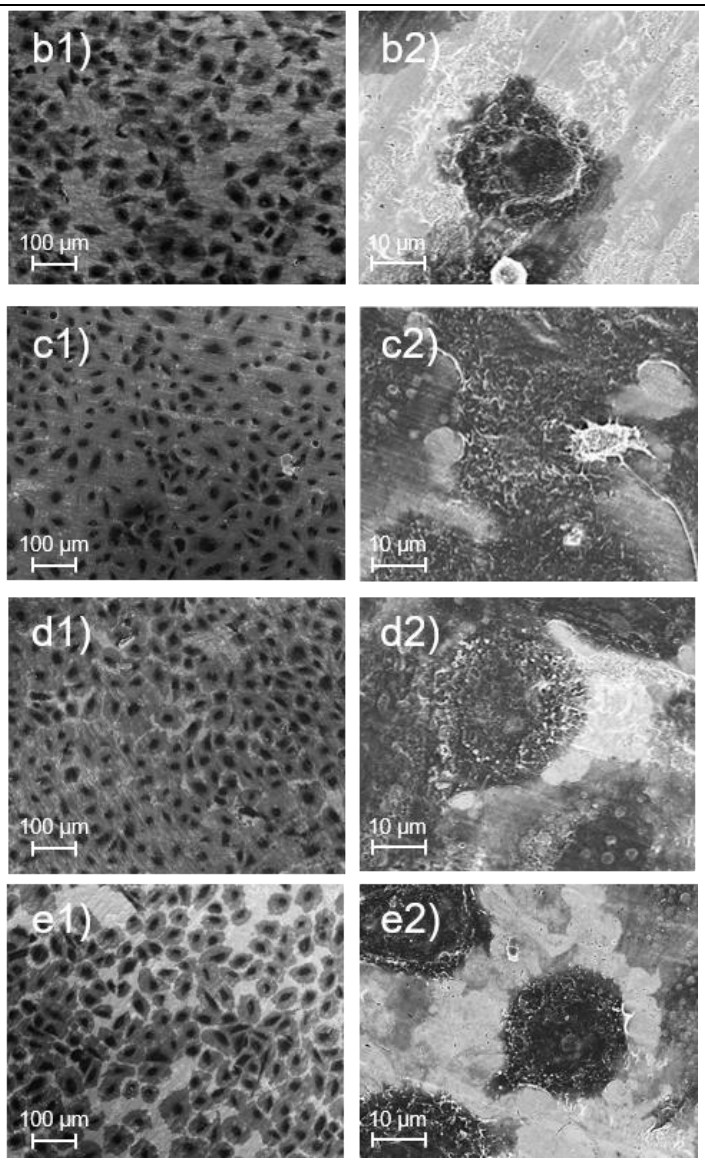

Fig 17. SEM images of epithelial cells after 3 hours of incubation
(a1, 2)ST, (b1, 2)NT, (c1, 2)ST-CL, (d1, 2)NT-CL, (e1, 2)NT-EPF

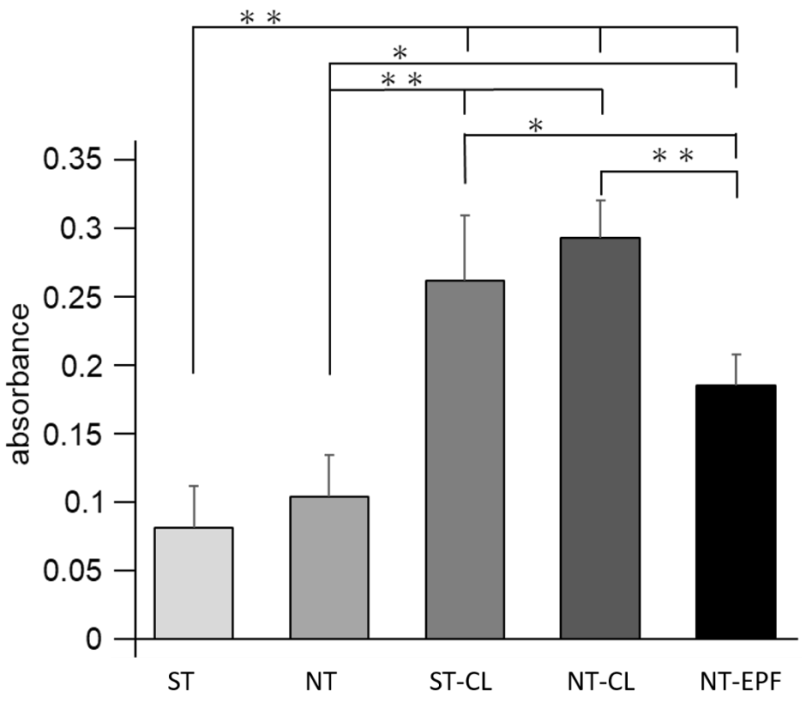

Fig 18. Relative amount of epithelial cell on each group surfaces

Promoting Fibroblast Attachment

The mode of fibroblast attachment on each treated titanium surface was identified by SEM ultrastructure (Fig. 19). On NT surfaces with and without Col-I coatings, fibroblasts demonstrated a more elongated spindle-cell morphology compared to the more rounded shapes on ST surfaces. The elongated cells extended filopodia-like process, as periodontal fibroblasts did on dentin surface.(66, 67) Furthermore, significantly higher number of fibroblasts were seen on NT-EPF than on NT-CL. (Fig. 20) On NT-EPF, fibroblasts showed the typical filopodia extension (Fig. 19e2) suggesting

focal adhesion kinase dependent migration and cell growth.(68) When SEM image was taken at a 30 degree tilted angle (Fig. 19e2), filopodia linked to NT-EPF. This implied that fibroblasts would form ligamental network with the NT-EPF surface via their extracellular collagen matrix.

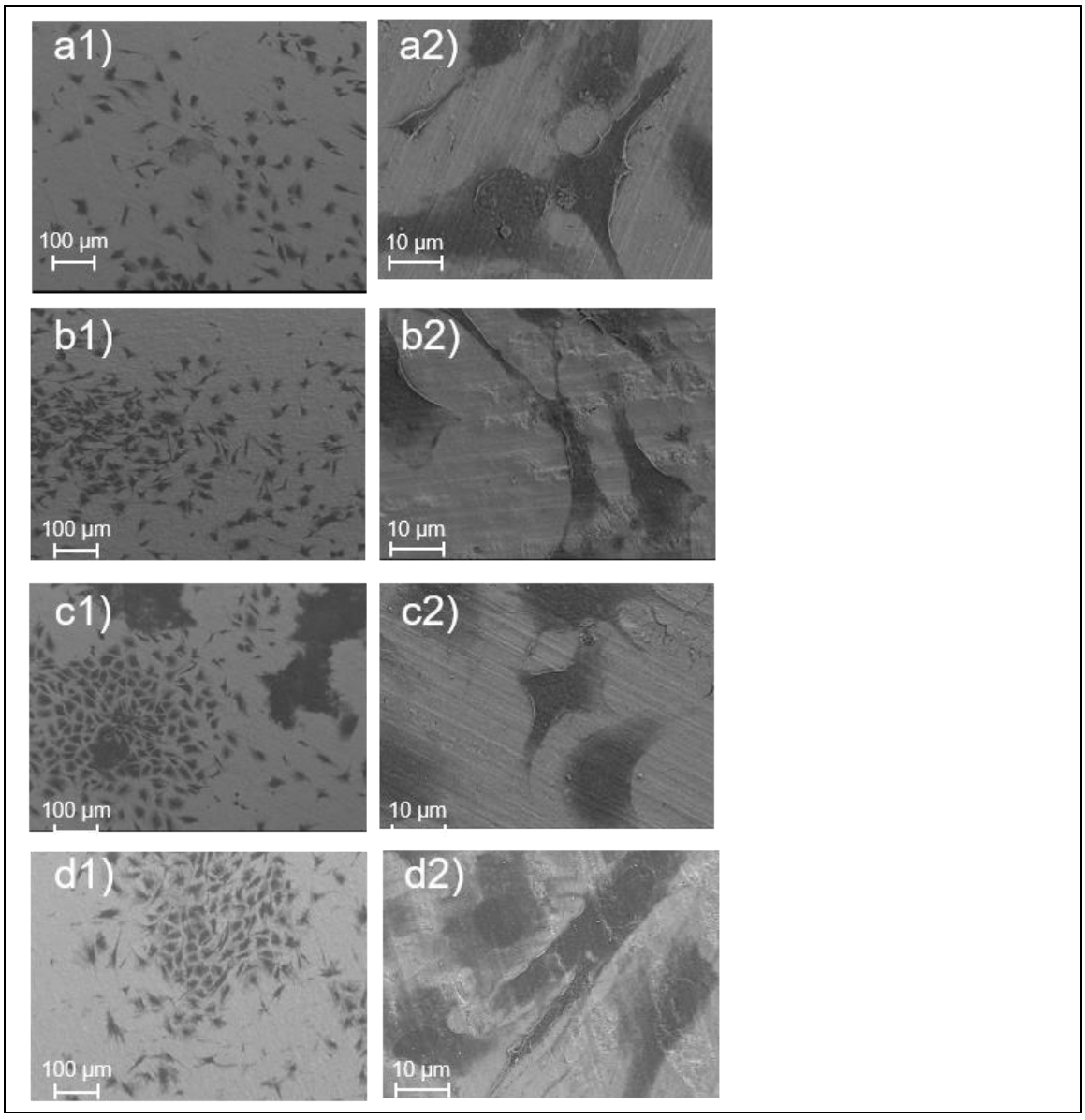

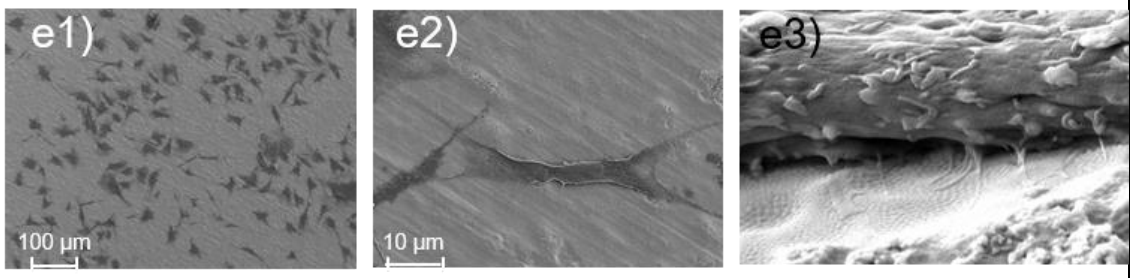

Fig 19. SEM images of fibroblasts after 24 hours of incubation
(a1, 2)ST, (b1, 2)NT, (c1, 2)ST-CL, (d1, 2)NT-CL, (e1, 2, 3)NT-EPF.

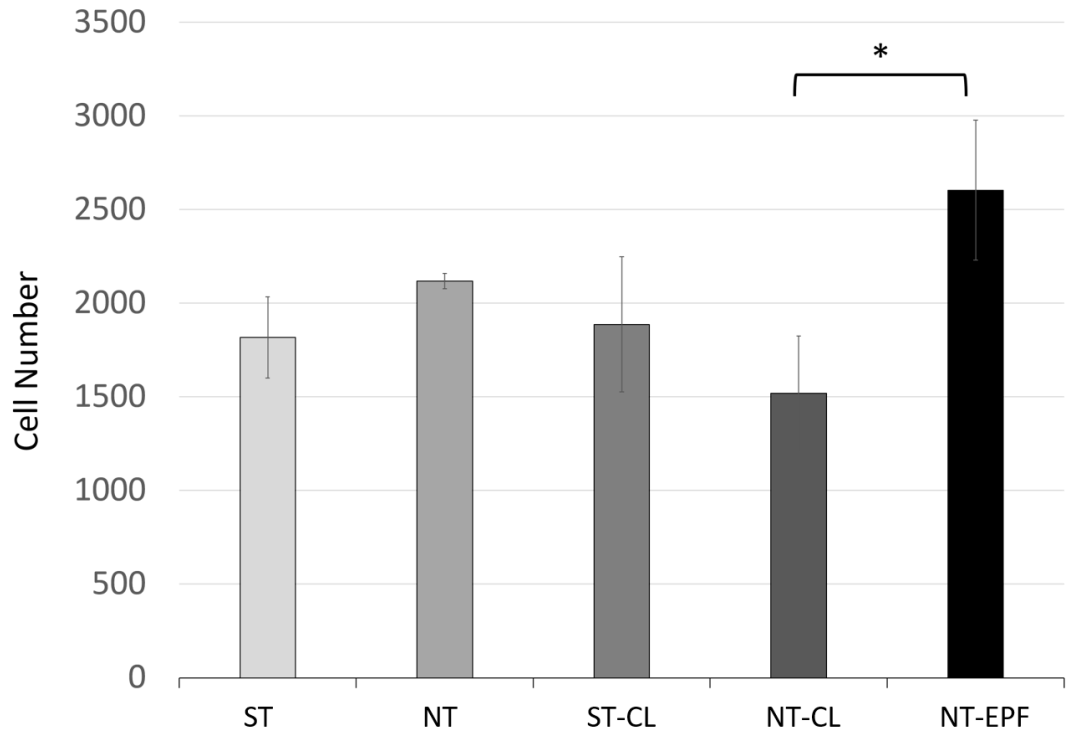

Fig 20. Number of fibroblasts in each group at 24 hours (*p<0.05)

Platelet Activation and Growth Factor Release

Examining the effects of different surfaces on platelet aggregation and activation, we found that the NT-EPF surface was able to induce early platelet aggregation and activation as early as 30 minutes. (Fig. 21) ELISA assay for PDGF-AB and TGF-β gave us more insight into the influence of different surfaces in terms of topography and Col-I coating. For PDGF-AB concentration, we found that all surfaces with Col-I coating, regardless of surface topography or binding methods, had a significant increase from 30 min to 3 hours when compared to non-coated surfaces. (Fig. 22) Examining the results at 30 minutes and one hour, the nanotube topography also influenced PDGF-AB release; however, the effect was not as significant as Col-I coating. On the other hand, for TGF-β concentration, we found that all NT surfaces, regardless of the presence of Col-I coatings, had an instant effect on TGF- β release, as exemplified by the significant concentration of TGF- β at 30 minutes compared to ST surfaces. (Fig.23) Compared to PDGF-AB, the overall concentrations of VEGF, another growth factor known to promote angiogenesis, were minimal, with a significant increase when compared to pure smooth titanium (ST) surface at 3 hours. (Fig.24) Looking into TNF-α, an inflammatory cytokine, the overall concentrations were low across all samples with Col-I coatings showing a slightly elevated concentration at 1 hour. (Fig.25)

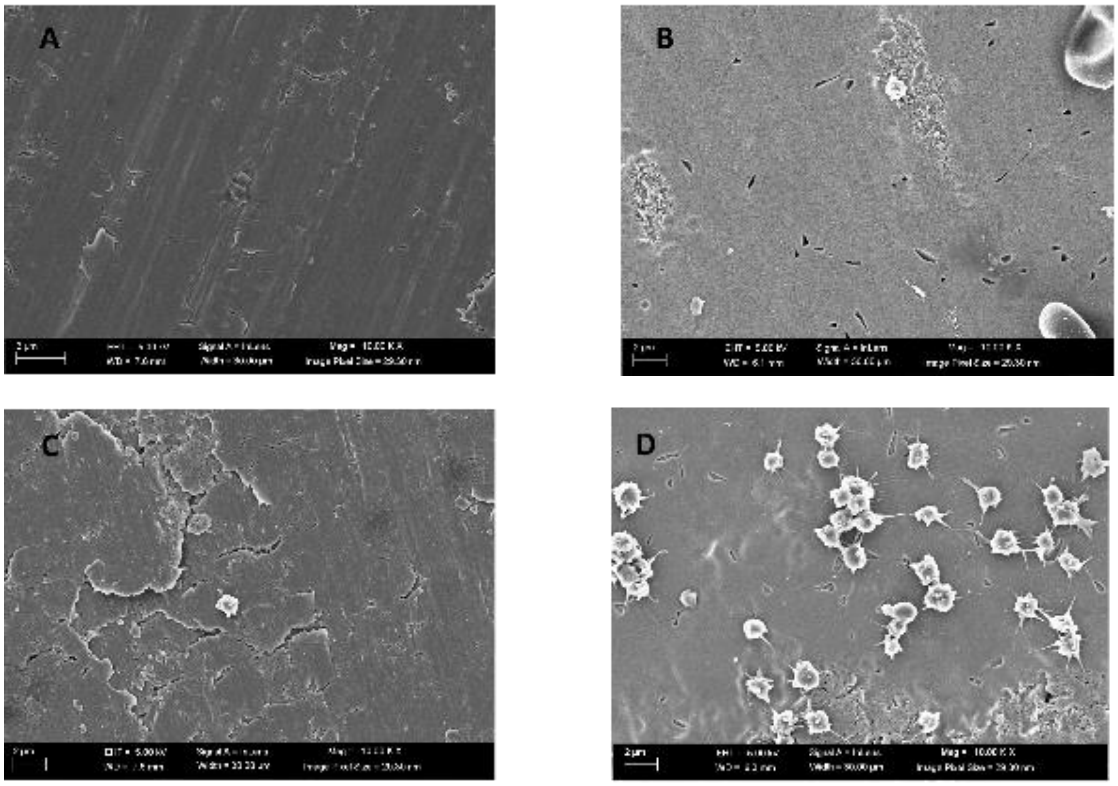

Fig 21. SEM images of Samples after 30-min Platelet-Rich Plasma (PRP) Incubation
A: ST; B: NT; C: ST-CL; D: NT-EPF

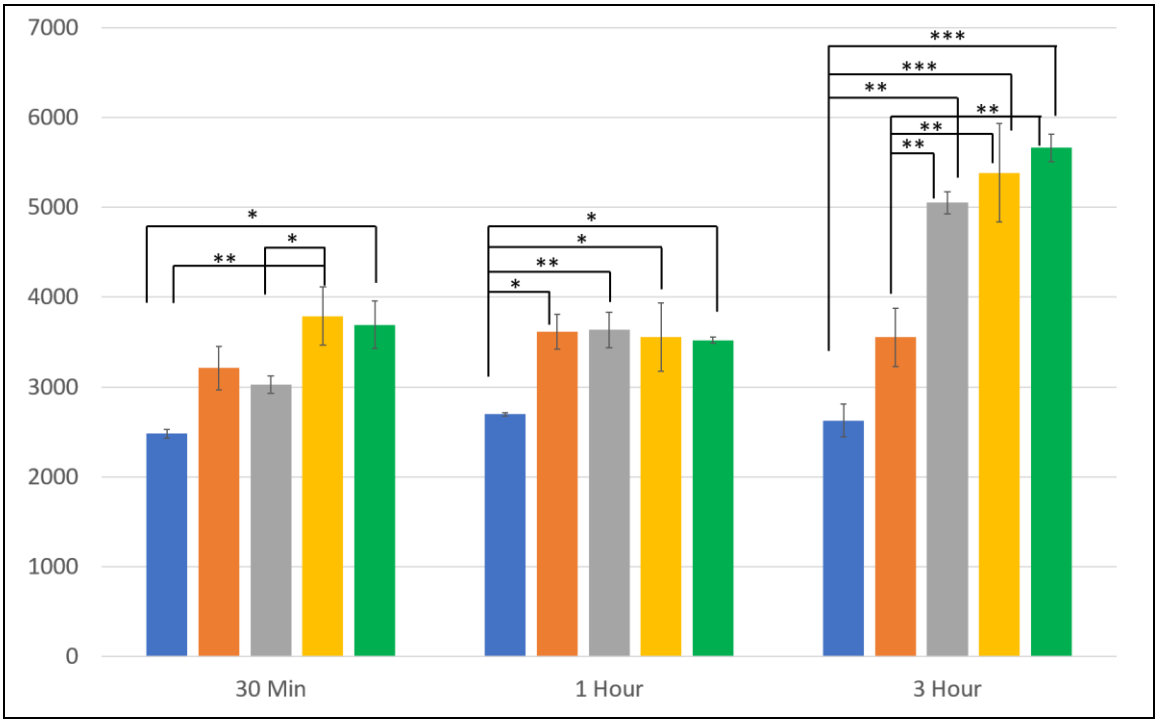

Fig 22. ELISA results for PDGF-AB concentration (pg/mL)
At 3 hours, all collagen-treated surfaces (CL and EPF) have significant increase in PDGF-AB concentration. (Blue: ST; Orange: NT; Grey: ST-CL; Yellow: NT-CL; Green: NT-EPF) (*p<0.05; **p<0.01; ***p<0.0001)

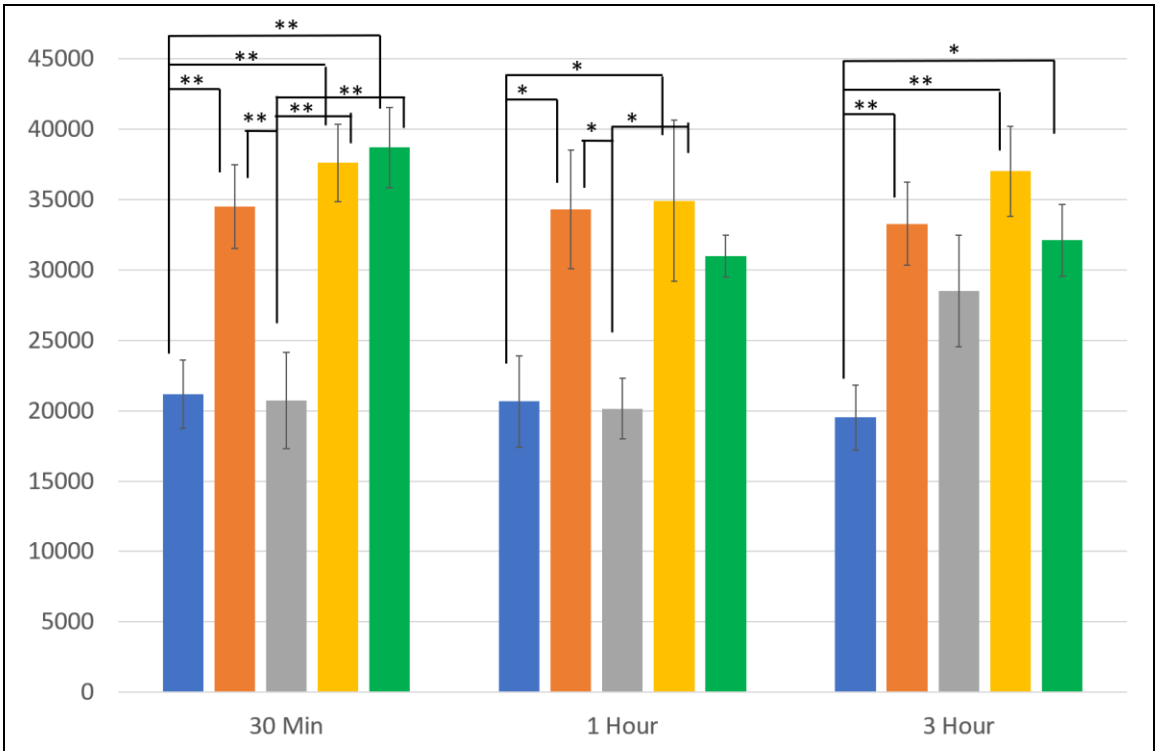

Fig 23. ELISA results for TGF-β concentration (pg/mL)
At 30 minutes, sample surfaces with nanotube topography significantly contributed to increase in TGF-β level (Blue: ST; Orange: NT; Grey: ST-CL; Yellow: NT-CL; Green: NT-EPF) (*p<0.05; **p<0.01; ***p<0.0001)

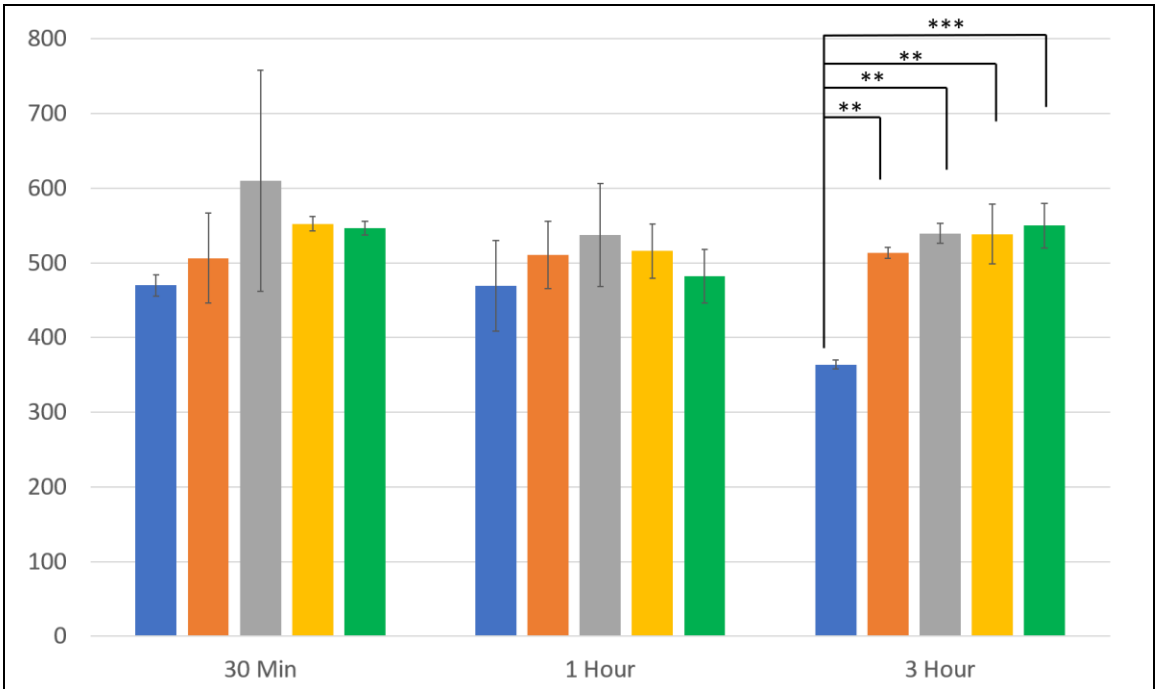

Fig 24. ELISA results for VEGF concentration (pg/mL)
At 3 hours, surface treatment (both topography and Col-I coating) had an increase amount of VEGF release. (Blue: ST; Orange: NT; Grey: ST-CL; Yellow: NT-CL; Green: NT-EPF) (*p<0.05; **p<0.01; ***p<0.0001)

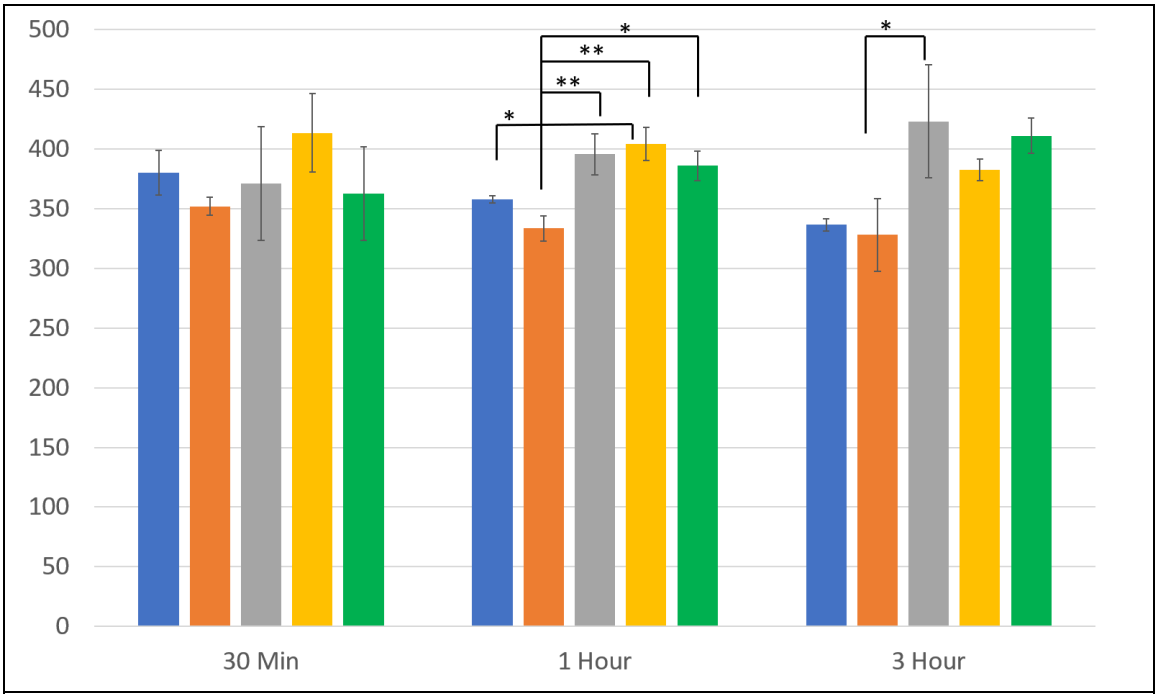

Fig 25. ELISA results for TNF-α concentration (pg/mL)
Col-I coating had an effect on the TNF-α concentration at 1 hour. (Blue: ST; Orange: NT; Grey: ST-CL; Yellow: NT-CL; Green: NT-EPF) (*p<0.05; **p<0.01; ***p<0.0001)

Platelet-Induced Fibroblasts Migration

At the end of 3-hour PRP incubation, a fibrin gel could be seen on all the surfaces. When these samples were place facing down into a culture well with fibroblasts in the "Down" assay model, we found that the fibrin gel remained visible at 24 hours and fully dissolved at 48 hours. The cell count results indicated that the NT-EPF surface significantly attracted fibroblasts to migrate toward the surface at both 48 and 72 hours. (Fig. 26) The effect could be explained by the high surface hydrophilicity, release of PDGF-AB and TGF-β. Interestingly, the Col-I coating through CL method did

not seem to have the same effect the fibroblasts migration; in fact, the NT-CL surface had the least amount of viable cells at 72 hours.

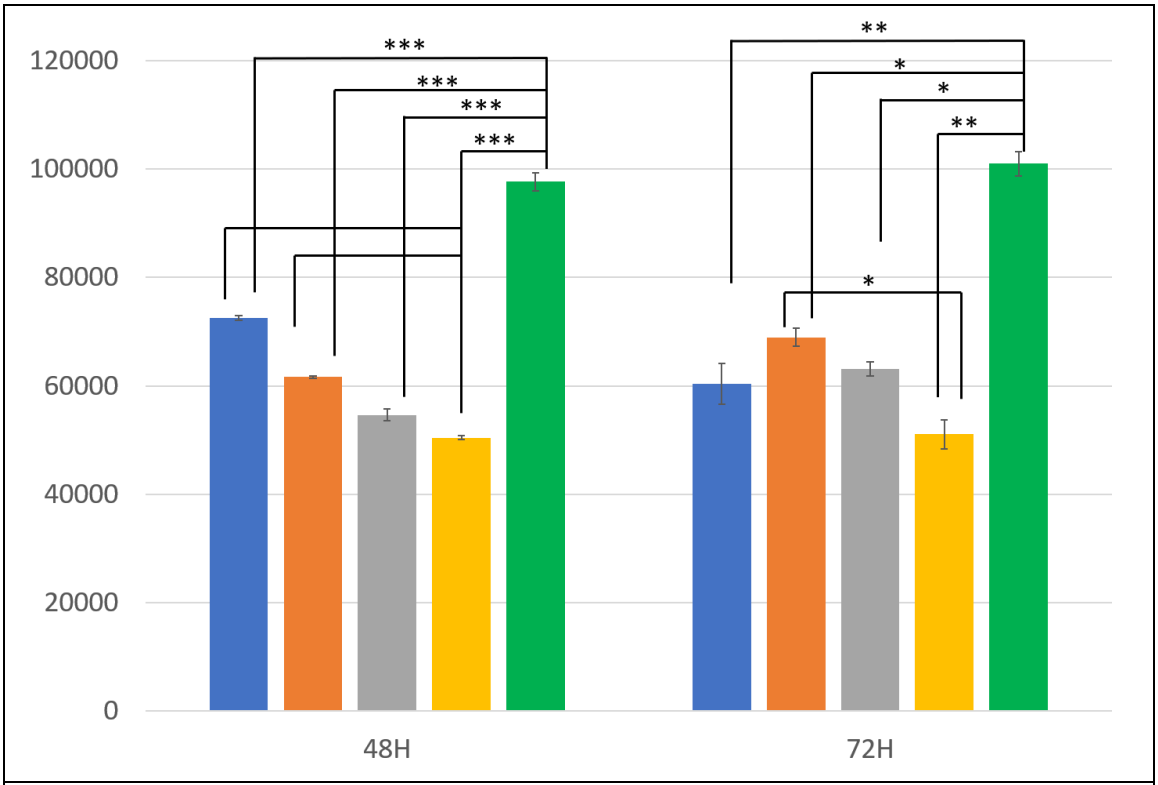

Fig 26. Cell migration assay in a down model
(Blue: ST; Orange: NT; Grey: ST-CL; Yellow: NT-CL; Green: NT-EPF) (*p<0.05; **p<0.01; ***p<0.0001)

III. Discussion

Many researchers have studied the interaction between nano-scale surface topography and various cell types in terms of cell adhesion, proliferation and migration. It has been shown that diameters of smaller than 100 nm are optimal for enhanced

cellular adhesion due to increased surface energy.(69, 70) The dental implant abutment is a transmucosal device that interacts with both the keratinocytes and fibroblasts. A previous study has shown epithelial cells and fibroblasts respond differently to nanoscale topography. Smith et al showed increased dermal fibroblast and decrease epidermal keratinocyte adhesion, proliferation and differentiation on TNT arrays with a diameter of 70-90 nm and a length of 1-1.5 μm.(71) Our results with the epithelial and fibroblasts attachment assay somewhat corroborated with previous research.

In the epithelial cell attachment assay, our result did not show statistical differences in cell attachment between ST and NT surfaces, not treated with collagen. These results did not contradict findings by Smith et al because the depth of our nanotubes were much less than the 1 μm used in their study and epithelial cells required at least 100 nm groove depth to induce a response.(72) We observed a greater numbers of cells on all Col-I treated surfaces. However, the cell morphologies were different among the samples. The cells adhered with spreading plasma membrane with pseudopod like stretching both smooth and nanotube surfaces treated with chemical linking collagen (ST-CL, NT-CL). (Fig. 17c1, c2, d1, d2) By contrast, the cells sparsely localized and did not spread their plasma membrane on the nanotube surface treated with EPF Col-I binding. (Fig. 17e1, e2) The epithelial cells wrapped over the horizontal collagen layer as they do on a subcutaneous connective tissue layer such as endothelial

cells. The complex nano-sized surface substratum coupled with perpendicularly oriented collagen influenced epithelial cell behavior and slow epithelial cell migration substantially.

Although no differences in fibroblasts cell numbers were observed at the 3-hour mark, our result showed a statistically significant higher number of fibroblasts on the NT-EPF surface in the 24-hour fibroblasts attachment assay. Morphology wise, more spindle-shaped cells were observed on all the NT surfaces. As demonstrated in the high magnification (50k) SEM image taken at 30 degree tilted angle, the fibroblasts cell attached tightly to the nanotubes and extended fibrillar processes to the surface. (Fig. 19e3) Our findings are in agreement with previous studies showing a positive influence of nano-topography on fibroblasts behavior.(73) Furthermore, the behavior of the fibroblasts on the NT-EPF surface resembled what was observed on Laser-lok surface morphologically.(74) The laser-lok surface was shown to induce a direct connective tissue attachment in a human histological studies by Nevins et a.(9, 33)

After implantation of a biomaterial, blood-implant contact heralds the biological evens that occurs in the wound healing process. Therefore, early response of blood platelets to the titanium surface would significantly influence subsequent biological healing through modulation of early tissue healing-microenvironments via the formation of a temporary fibrin matrix scaffolds and release of growth factors and cytokines. Our

SEM results showed that the NT-EPF surface was able to induce platelet adhesion and activation at 30 minutes when there were few platelets presents on other surface. Interestingly, in one study examining the effect of platelet adhesion on titanium oxide, the author concluded that a thinner oxide layer obtained by H_2O_2 positively influenced the number of adhered platelets while a thick oxide layer formed by heat treatment had a negative influence.(75) This may explain the reason why our NT-EPF surface showed an immediate effect on platelets. The post-anodization treatment with H_2O_2 and subsequent Col-I binding with the EPF method rendered the surface hydrophilic.

A study published by Park et al showed that nano-topography positively modulated the immediate blood platelet function and early macrophage immunoinflammatory response.(76) Our results indicated that the nano-topography has a marked effect on the release of TGF-β and a slight stimulatory effect on PDGF-AB which was masked by the greater influence of Col-I coatings. Since type I collagen is a known platelet activator, all Col-I treated surface, whether through CL or EPF, upregulated the release of PDGF-AB.(59) Both PDGF-AB and TGF-β are well known for their positive roles in fibroblasts migration and collagen synthesis. (55, 77, 78) In our "Down" culture model assay, we have shown that the combination of surface topography, chemistry and subsequent activation of platelet has a positive effect on the migration of fibroblasts.

Chapter 5. Establishment of Perpendicular Collagen Fiber Extension

I. Materials and Methods

A. Titanium Surface Fabrication

Four types of titanium surfaces were fabricated for the following experiments. For nanotube topography, the optimized setting as determined in the previous chapter was used. The four types of surfaces are: 1) smooth Ti (ST); 2) nanotube Ti (NT); 3) nanotube Ti with chemical linking Col-I (NT-CL) and 4) nanotube Ti with electrophoretic fusion of Col-I (NT-EPF).

B. Cell Culture and Maintenance of Mouse Fibroblast Cell Line (NIH3T3)

Mouse fibroblasts NIH3T3 cells were maintained in DMEM medium (Thermo Fisher Scientific) supplemented with 10% FBS at 37°C in 5% CO_2 and 95% atmospheric air. Cells maintained beyond 10 passages were used in the following experiments.

C. Fibroblast (NIH3T3) Cell Culture Insert Model

In a 12-well plate with cell culture insert with mesh pore size of 3 μm (Thermo Scientific, USA), specimens with four different types of surfaces as described above were placed at the bottom of the wells with and without addition of fibroblasts into the culture insert. (Fig. 27) Fibroblasts were seeded at 100k per 1 cm^2 for a total working volume of 1 μl per culture insert according to manufacturer's protocol for 3 days. At the

end of the incubation period, the specimens were carefully rinsed with PBS and processed for either SEM (Zeiss Ultra55; Zeiss) or immunofluorescent staining with a FITC-conjugated Collagen I antibody (biorbyt, Cambridge, UK). Briefly, the specimens were first fixed with 4% PFA for a maximum of 20 minutes at room temperature. Afterwards, the specimens were washed with PBS for 5 minutes for a total of 3 changes. Unspecified staining was avoided by blocking the specimen with 1% BSA in PBS for 1 hour. Specimens were washed again with PBS for 5 minutes for a total of 3 changes. Finally, the specimens were incubated with the antibody diluted to a working concentration of 1:200 with an immunoreaction enhancer solution (Can Get Signal®, TOYOBO, Japan) for at least 16 hours at 4^0C. The specimens were gently rinsed and mounted with Fluoroshield mounting medium (abcam, USA) and a cover glass. The specimens were imaged with a multiphoton confocal microscope (LSM 710, Zeiss, Oberkochen, Germany) either on the day of or within 3 days.

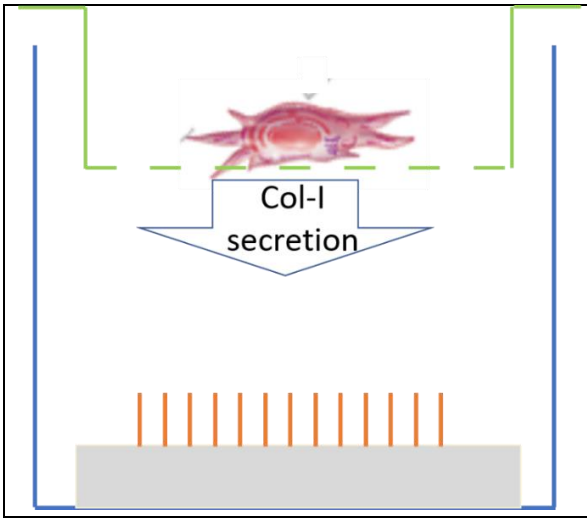

Fig 27. Schematic Representation of Fibroblast Culture Insert Model

D. Acellular Collagen Extension Model in Fibroblast-conditioned Medium

When NIH3T3 cells reached confluence, the culture medium was collected. To remove cells contained in the medium, it was centrifuged, and the supernatants were transferred into a new tube. Stock Col-I solution (3 mg/mL) was added to the medium to a final concentration of 0.3 mg/mL. In a 24-well plate, specimens with four different types of surfaces as described above were placed at the bottom of the wells with 1 µl of the collagen-spiked, fibroblast-conditioned medium added. The plate was placed in a temperature-controlled shaker/incubator at 37^0C for at least 16 hours. At the end of the incubation period, the specimens were processed for SEM (Zeiss Ultra55; Zeiss) examination.

E. Acellular Collagen Extension Model with Collagen Gel

Collagen gel was prepared by using a stock type I collagen solution (3mg/mL, pH= 3, Atelocollagen: Atelo Cell® IPC-30, KOKEN, Japan). All reagents as well as culture plates were kept on ice during collagen gel preparation. For a collagen gel with a final concentration of 1 mg/mL, 10X PBS, distilled water and stock collagen solution were mixed with a volume ratio of 1:5:3. To adjust the final pH to 7.4, 0.1 N NaOH was used to titrate the mixture. Specimens with 4 different surfaces as mentioned above were placed at the bottom of a 24-well plate and 200µl of the prepared Col-I mixture was added to each well. The plate was sealed with parafilm and placed in a cell incubator at 37^0C to allow for gelation for at least 16 hours. At the end of the gelation period, the samples were fixed with 4% PFA and processed for either SEM (Zeiss Ultra55; Zeiss) or multi-photon laser scanning microscopy (Olympus Fluoview FV1200, Japan) examination.

F. Cellular (NIH3T3) Collagen Extension Model

Specimens with 4 different surfaces as mentioned above were placed at the bottom of a 24-well plate. NIH3T3 cells were seeded at 50k per 1 mL into each well. After the cells were settled for 24 hours, the medium was aspirated, and new culture medium supplemented with L-ascorbic acid (50 mg/mL) was added. The supplemented medium was replaced every 2 days for a total of 8 days. At the end of the incubation

period, the specimens were gently rinsed with 3 changes of PBS and fixed with 4% PFA for 20 minutes. The specimens were processed for either SEM (Zeiss Ultra55; Zeiss), multi-photon laser scanning microscopy examination (Olympus Fluoview FV1200, Japan) or confocal Raman spectroscopy (HORIBA, Kyoto, Japan).

G. Collagen Visualization and Analyses Modalities

a. Scanning Electron Microscopy (Zeiss Ultra55; Zeiss): Samples were fixed in 4% paraformaldehyde (PFA), washed in water, and dehydrated in ethanol series to 100% (75%, 80%, 85%, 90%, 95% and 100%, 20 min in each incubation). Prior to SEM examination, the surface was sputtered coated with 5 nm of gold.

b. Confocal Fluorescent Microscopy (LSM 710, Zeiss, Oberkochen, Germany): Samples were fixed in 4% PFA and stained with FTIC-conjugated collagen-I antibody according to protocol. The images were taken with a 20X objective. The 3D structure was captured by using the Z-stack function. The images were processed with ImageJ software with 3D plug-in.

c. Second Harmonic Generation (SHG) with Multi-photon Laser Scanning Microscopy (Olympus Fluoview FV1200, Japan): Samples containing cells were fixed in 4% PFA for 20 minutes and then stored in PBS while

acellular samples were stored in PBS without fixation. For cellular samples, immunofluorescent staining was performed with FTIC-conjugated collagen-I antibody according to protocol. The second harmonic generation (SHG) imaging was obtained with a 20X 1.2 NA water-immersion objective and a tunable Mai Tai laser source tuned to an excitation wavelength of 910 nm to produce backward SHG signal at 455 nm. The images were processed with IMARIS software (Bitplane, Switzerland).

d. Confocal Raman Spectroscopy (HORIBA LabRam Evolution, Kyoto, Japan): Samples were fixed with 4% PFA and stored in PBS at 4^0C until observation. The Raman system consists of an upright microscope equipped with 10x, 20x LWD, 50x LWD and 100x objectives. A continuous laser beam was focused down to a micrometer sized spot on the sample through the microscope. A green laser (λex = 532 nm) with 100% output was used in combination with a 50x objective. To properly obtain the collagen signal at the titanium surface layer, the aperture was adjusted down to 100 for better Z resolution. The spectra were acquire using a synapse CCD detector behind an 800 mm spectrometer with a 600 blaze grating. Using a polarization analyzer, regions of interest were scanned at different angles of polarization laser from 0~180^0 (30^0 intervals). Each

Raman spectrum was collected with an acquisition time of 20 s, and 2 accumulations. The spectra analysis was performed in the fingerprint range (700-1800 cm^{-1}). Raman spectra were preprocessed using the LabSpec 6 Software (HORIBA, Japan) for baseline correction and to remove autofluorescence.

H. Statistical Analyses

For Raman multivariate analysis, the PLS tool box plug-in for MATLAB (Eigenvector Research, Inc, WA, USA) was used to conduct principle component analysis (PCA) as well as spectral normalization.

II. Results

Endogenous and Engineered Collagen Integration

To answer the question of whether or not Col-I secreted by fibroblasts could integrate with the Col-I coatings on specimen surfaces, a cell culture insert model with a mesh pore size of merely 3 µm, which allowed the passage of cell-secreted collagen but not the migration of the cells themselves, was utilized. After 3 days of incubation, while collagen could sparsely be observed on the control surfaces (T, NT and NT-CL), both SEM and confocal microscopy results showed an increase amount of fibrinous tissues on NT-EPF surface. (Fig.28) Furthermore, confocal microscopy with Z scanning showed the

potential for perpendicular extension of collagen fibers. (Fig. 28-b3) This deposited layer is about 30 microns in thickness and seemed to follow the outline of the nanotube structures.

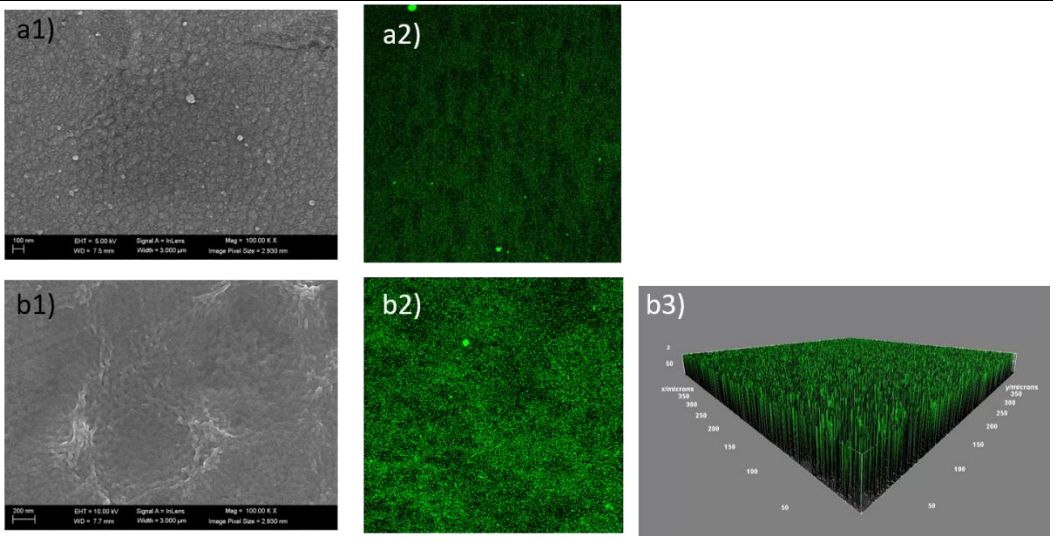

Fig 28. SEM and Confocal Microscopy Result of Cell Culture Inserts Incubation
Upper row: SEM (a1) and confocal microscopy (a2) images of NT-EPF with DMEM medium but no cells incubation for 5 days
Bottom row: SEM (b1) and confocal microscopy (b2) images of NT-EPF of with DMEM as well as cells inside culture inserts incubation for 5 days. (b3) is confocal z-stack image

Mode of Collagen Insertion

To elucidate the mode of Col-I extension and insertion onto the NT-EPF samples, both acellular and cellular systems were employed. When Col-I was added into fibroblast-conditioned medium as a source of collagen cross-linking enzyme, lysyl oxidase, and incubated with Ti specimens overnight at 37^0C on a rocking table, we found

that collagen fibers with the signature 67 nm striations were formed and deposited onto all titanium sample surfaces. (Fig. 29a) Higher SEM magnification image revealed that underneath the largely parallel networks of collagen fibers, small fibrils extending perpendicularly from the NT-EPF surface was found. (Fig. 21b). When the samples were fixed but left hydrated in PBS for SHG imaging, we located a small isolated region with evidence of obliquely-oriented collagen fibers form the NT-EPF surface. (Fig. 29c)

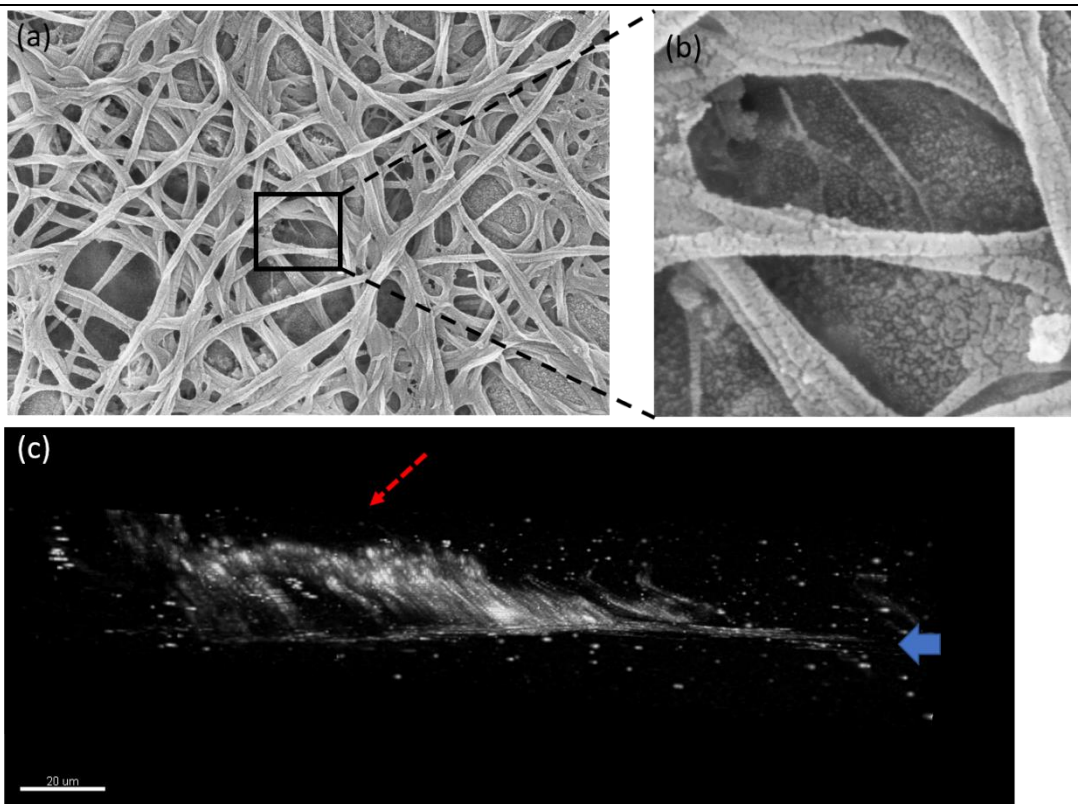

Fig 29. SEM and SHG images of Col-I on NT-EPF surface
(a) SEM image of NT-EPF surface after incubation in Col-I fibroblasts-conditioned medium overnight. (b) 100k magnification of figure (a) captured an area where smaller fibrillar structures with direct insertion to the NT-EPF surface were observed. (c) SHG imaging captures collagen fibrils (red arrow) inserting obliquely to the NT-EPF surface (blue arrow)

When NIH3T3 fibroblasts were cultured with L-ascorbic supplementation at 50 mg/mL, cells began synthesizing a Col-I rich extracellular matrix. Confirmed by both immunofluorescent staining with FITC-conjugated collagen I antibody and the intrinsic SHG collagen signal (white), 3D reconstruction of Z-stack image of fibroblast extracellular matrix on all sample surfaces surface revealed that about 20 µm from the metal surface, cells formed a robust collagen sheet on the top that lies parallel to all sample surfaces. (Fig.30) Focusing on the NT-EPF surface, we noticed that the 20 µm space in between the cell collagen sheet layer and the titanium surface seemed to be devoid of both fluorescent and SHG signals. (Fig. 31a) Just like what was observed previously with samples incubated in acellular system, SEM images also revealed that underneath the horizontally aligned layer, small fibrils seemed to insert obliquely into the NT-EPF surface. (Fig. 31c)

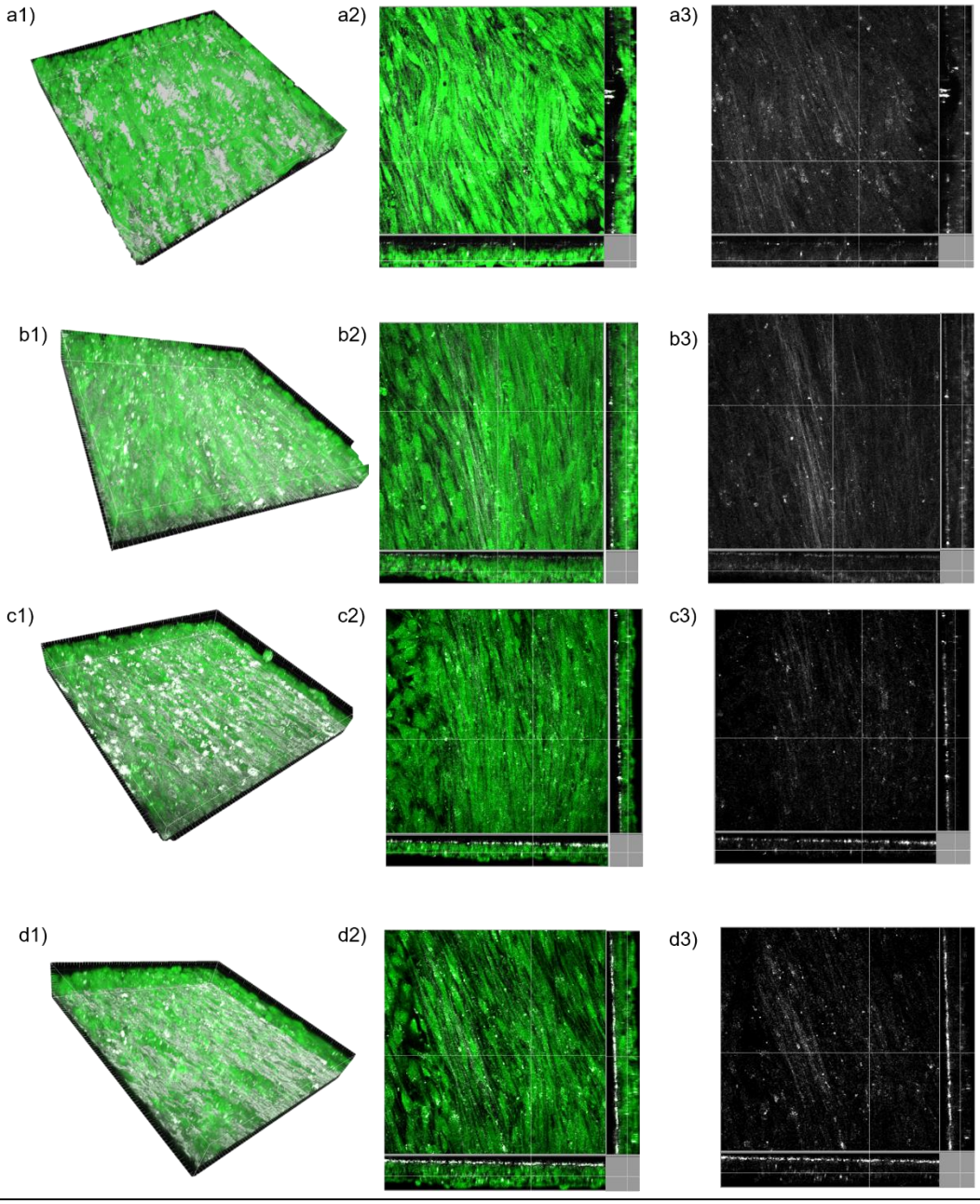

Fig 30. SHG images of Fibroblasts deposited Col-I on Titanium Surfaces
(a) ST (b) NT (c) NT-CL (d)NT-EPF

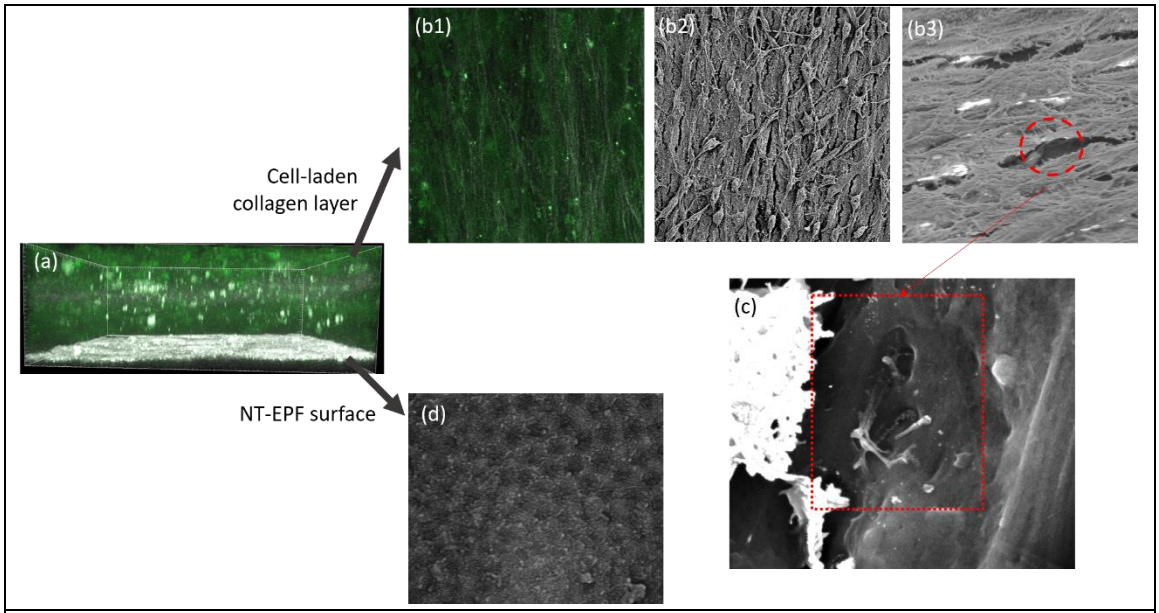

Fig 31. Cell Extracellular Matrix Structural Imaging with SHG and SEM
(a) Z-scan of cell extracellular matrix structure on NT-EPF
(b1-3) SHG with GFP staining and SEM images of the top cell-laden collagen layer
(c) SEM images of the gap between the cell-sheet layer and the NT-EPF surface, noticed the oblique fibrillar attachment to the NT-EPF surface
(d) SEM image of the NT-EPF surface after carefully peeling off the cell-formed layer

To further elucidate the collagen structures in the 20µm gap as seen in Fig. 31, Raman spectroscopy was utilized to confirm the presence of collagen in the gap and to extrapolate the orientation of the collagen fibrils. The polarized Raman anisotropic response of collagen fibers have long been investigated to map the 3D orientation of collagen in tissues.(79) Following methods and theory set forth by Masic et al and Bergholt et al, we first applied a principal component analysis (PCA) for all 20 sets of spectra (n=5 per groups) in the Col-I fingerprint range (800-1800 cm^{-1}) to extract the anisotropic spectral variation.(80-82) We confirmed that the Amide I peak (1600-1700

cm^{-1}) showed the highest anisotropic scattering and thus used it to estimate collagen orientation. (Fig. 32)

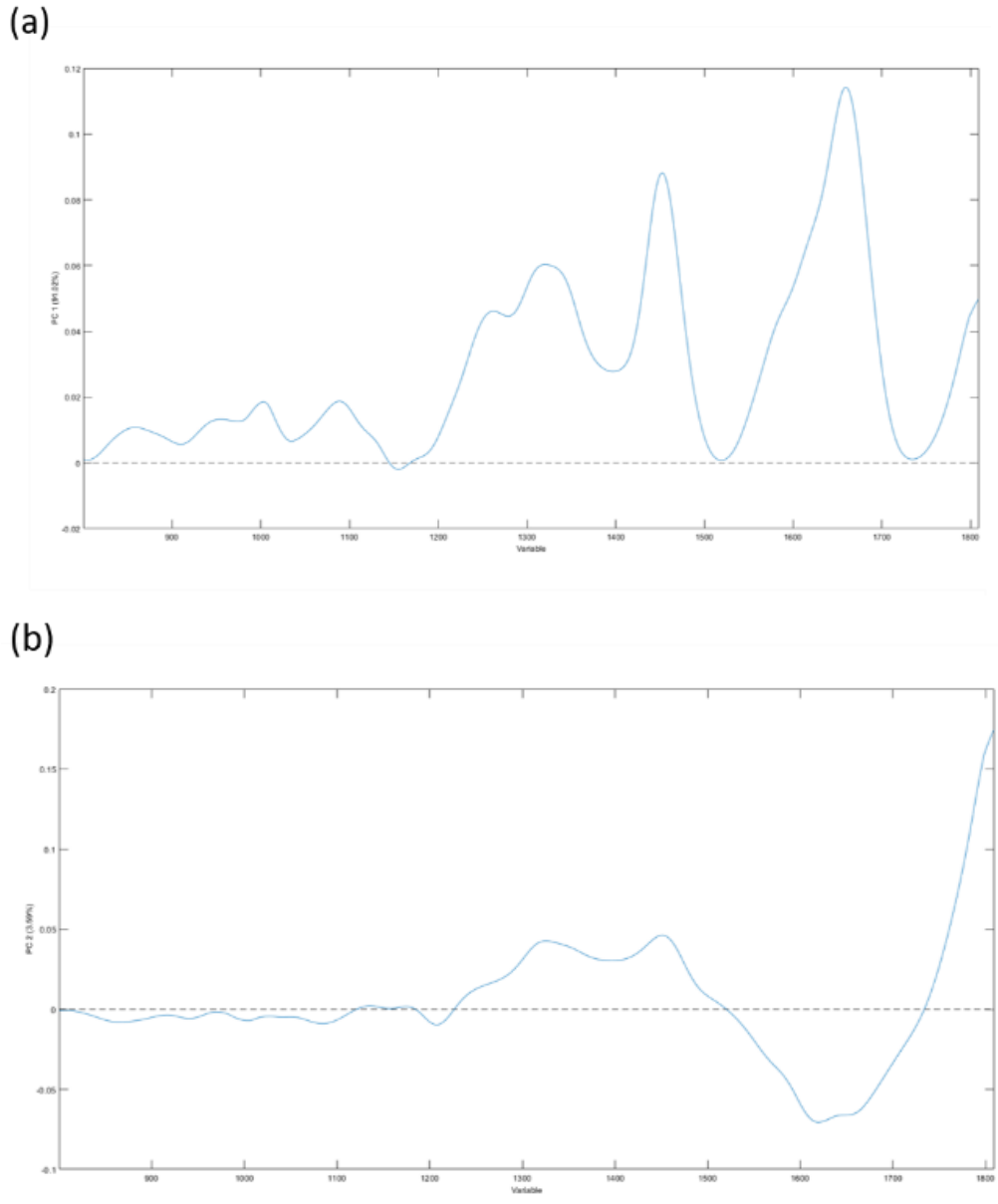

Fig 32. Principal Component Analysis (PCA) loading

Five regions were randomly selected on the samples (T, NT, NT-CL, NT-EPF); each region was scanned both at the titanium surface level and 20 µm above. For each scan, polarized confocal Raman spectra was measured in an 180^0 rotation (30^0 interval). The chemical images were reconstructed by integrating over defined Raman shift regions in the spectrum using s sum filter (for amide I band, the spectral region used was 1600-1700 cm^{-1}). The filter calculated the intensities within the chosen borders and the background was subtracted by taking the baseline from the first to the second order. These operations were performed according to standard Raman spectral processing protocol with the native Raman software, LabSpec6 (Horiba, Japan). By averaging the spectrum of the Amide I (1600-1700 cm^{-1}) peak from all scans taken at each region, we found that the NE-EPF surface data deviated from all other regions. (Fig. 32) To further elucidate the differences and to extrapolate information related to collagen orientation, we followed the method proposed by Schrof et al to perform a non-linear least square fitting procedure using the following equation:

$$\mathbf{I = pr1(1+pr2(cos2(x-pr3)))}$$

where I is the amide I intensity response, pr1 the mean intensity, pr2 the amplitude of the fitting curve, x the polarization angle of the laser (radians), and pr3 the phase shift.(81)

Since the amplitude of the fitting curve directly related to the anisotropic response of the amide I band, a one-way ANOVA was done for the pr2 parameter and it was found that the amplitude of the fitting curve for NT-EPF was significantly lower than other surfaces.(Fig. 33) While definite conclusion to the exact orientation of the collagen insertion at the metal surface level could not be determined. It was clear from SEM and SHG images that the collagen layer was clearly visible at 20µm above the titanium surface oriented primarily in a horizontal fashion relative to the surface. Therefore, we can conclude that the collagen detected at the NT-EPF metal surface level had an orientation that differed from all others and could potentially be attaching to the titanium metal surface directly in a perpendicular or oblique fashion.

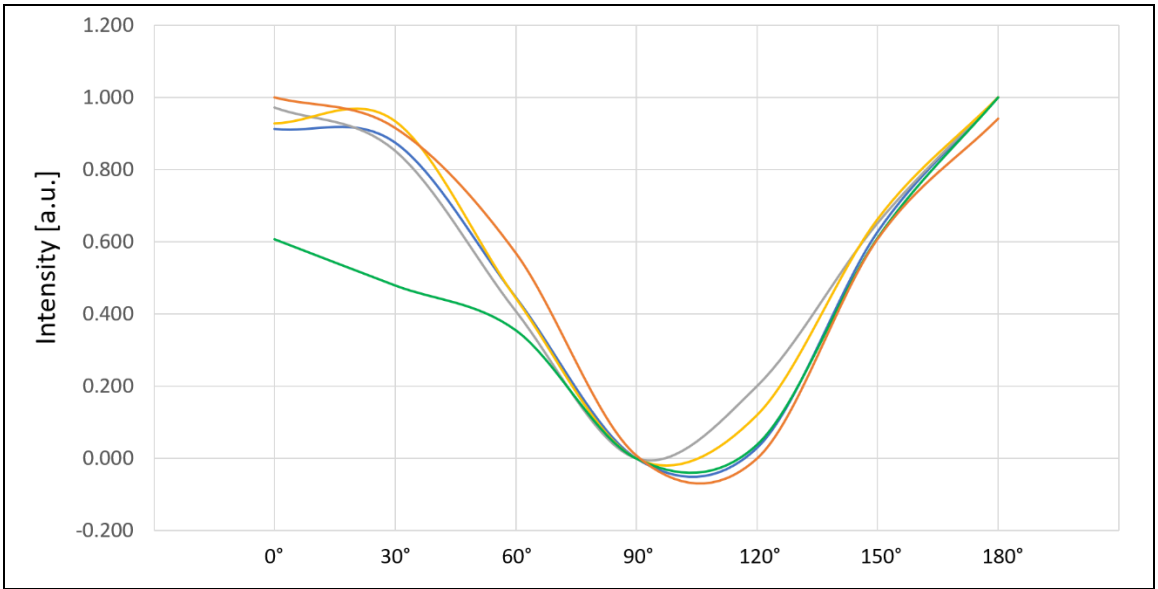

Fig 32. Raman Spectra Intensity of Amide I
Each line represented the Amide I intensity measured as the laser beam excited the sample at different angles. The NT-EPF (Green) clearly deviated from all other sample

curves. Others (ST, ST-CL, NT-CL) all resembled the average line of the 20 µm level (Orange). (Blue: ST; Grey: ST-CL; Yellow: NT-CL; Green: NT-EPF; Orange: 20µm above surface)

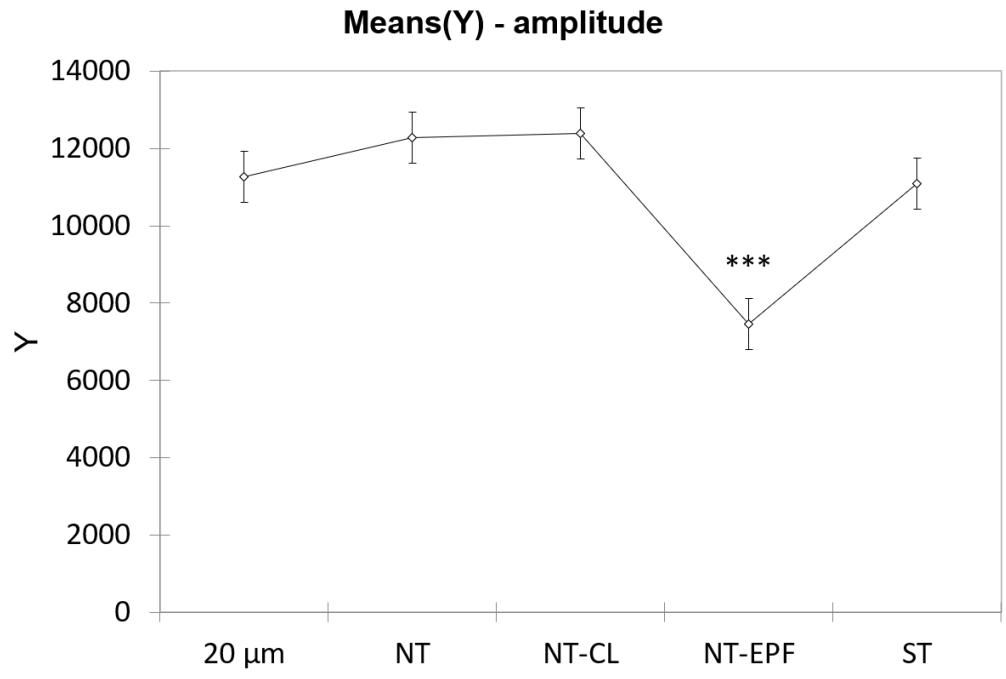

Fig 33. Average Amplitude of the Fitting Curves for Each Surface
The amplitude of the fitting curve for NT-EPF is significantly lower than other surfaces.

III. Discussion

The biologic soft-tissue seal around the dental implant is critical to its long-term prognosis. As many studies have pointed out, a key difference between the connective tissue attachment around the natural tooth compared to that around a dental implant is the orientation of collagen fibers.(83, 84) The peri-implant connective tissue can be

divided into two zones; the outer zone is cell-rich and well vascularized with fibers running in many different direction while the inner zone consists of numerous dense collagen fibers running close to the implant surface, mostly in a parallel direction.(32) This inner zone, rich in fibers with few scattered fibroblasts is about 50-100 mm thick and is in direct contact with the implant/abutment surface. The peri-implant mucosa, in a way, resembles scar tissue and exhibits an impaired resistance towards bacterial colonization.(35, 85)

Various models have been utilized to examine the implant-soft tissue interface, including *in vitro* studies, animal studies and human studies. While en bloc tissue histology is considered the best method, an *in vitro* study using monolayer cell culture model is conducted as a prerequisite to *in vivo* evaluation and to quickly evaluate cytotoxicity and cell behavior towards the new implant material. Previous studies have utilized immunostaining, scanning electron and/or fluorescent microscopies to study cell shape morphologically. The gene and protein expressions for cell adhesion and attachment have also been carried out.(10, 74) In this study, we employed two *in vitro* models and several imaging technologies to elucidate what goes on at the titanium surface.

The primary goal of this study was to establish a stable Col-I coating with sufficient protrusions from the *ex vivo* engineered titanium nanotube array to serve as a

priming site for subsequent self-assembling of cell-secreted collagens. In the cell-insert culture model, we simulated the in vivo condition whereby fibroblasts secreted proteins physiosorbed onto titanium surface. At the end of the incubation period at 3 days, we found, with anti-Col-I fluorescent staining, an increased amount of collagen on the TNT-EPF surface; furthermore, these collagens seemed to deposit following the nanotube outline underneath. On the contrary, we could hardly detect any collagens on ST, NT and NT-CL surfaces. Previous studies have investigated the relationship between different surface characteristics to the amount of protein absorption as it correlated to cell attachment and cell spreading.(86, 87) The ST and NT surfaces, both with a contact angle between 75 to 90 degrees, did not favor collagen absorption. Interestingly, collagen was also absent from the NT-CL surface which was pre-coated with collagen; this result confirmed yet again that the CL-immobilized collagen was less stable and possibly more susceptible to degradation by collagenases in the culture system. Another speculation is that the parallel collagen sheet deposited by the CL technique does not offer free collagen terminus for cross-linking while the perpendicular Col-I on the NT-EPF surface does.

To our knowledge, we are the first to employ second harmonic generation microscopy and Raman spectroscopy to investigate the interface between cell-secreted collagen-rich extracellular matrix and titanium surface. Both modalities have the

advantage of minimal sample preparations so that the delicate interface between cell-secreted collagen and the titanium is not disturbed. Second-harmonic generation (SHG) takes place when the electric field of the exciting light is sufficiently strong to deform a molecule. If the molecule is not symmetrical, the resulting anisotropy creates an oscillating field at twice the frequency, the second harmonic. Collagen is the strongest source of second harmonics in animal tissue due to its unusual molecular structure and its high degree of crystallinity. As clearly seen in Fig. 30 and 31, collagen could be detected by SHG with clear orientation information in the xy plane. Unfortunately, the technique is not without its limitation. It has been pointed out that collagen fibers with smaller diameters could not be detected by SHG.(88) Furthermore, since SHG will also take place at interfaces where there is a huge difference in refractive index, such as metal surfaces, we could not obtain information for collagen orientation at the titanium surface.(89)

Polarized Raman spectroscopy is a vibrational spectroscopy technique that can provide information regarding chemical composition in materials. It is based on the analysis of the inelastic scattering of light interacting with molecules in which frequency shift between the incident and the scattered light is associated with a particular vibration mode of a chemical bond. Confocal Raman microscopy is non-invasive and provides chemical information with high spatial resolution. The amide I band, mainly

due to C=stretching is highly anisotropic and thus has been selected to perform composition analysis in biological tissue such as bone.(90) Following the method proposed by Masic and others, we were able to detect differences in the anisotropic response of the Amid I band at the NT-EPF surface which suggested that collagen fiber attached to the NT-EPF surface in a non-parallel fashion.(81, 91)

Chapter 6. Conclusion and Future Work

In this study, we hypothesized that our modified surface with TiO_2 nanotube topography and type I collagen (Col-I) EPF coating would facilitate a biomimetic restoration of peri-implant soft tissue. The key innovation is the orientation of the fused Col-I. The nanotubes support the perpendicular insertion of Col-I monomers and these monomer projections, in terms, serve as the priming site for activation of in vivo healing process and subsequent assembly of direct connective tissue fibers.

We have optimized the conditions for fabrication of a titanium nanotube surface and the subsequent biofunctional coating with type-I collagen. The surface is bioactive as demonstrated in its potency to induce platelet activation. Its excellent fibroblasts affinity and resemblance to the Laser-lok surface in terms of fibroblast morphology in a 2D cell culture model suggested that we would be able to achieve similar results *in vivo*. For the first time, we demonstrated with Raman spectroscopy and other imaging modalities that fibroblast-secreted collagen fibers ligated with *ex vivo* engineered collagen on the titanium nanotube surface.

The study is not without its limitation as 2D *in vitro* techniques do not reflect the clinical situation and are not able to recapitulate the complex extra- and intracellular processes that occur in connective tissue attachment. We will move toward *in vitro* 3D culture model as well as *in vivo* mice animal model to further investigate the

establishment of a direct connective tissue attachment to our NT-EPF surface. Another potential pitfall of our study is the use of a xenogenic collagen (Bovine tendon). Therefore, we will also test our EPF technique with a chemically synthesized Col-I mimetic peptide comprised of –(Pro-Hyp-Gly)- tandem repeats.

We speculate that the orientation of the Col-I layer can affect the differentiation of mesenchymal cells. The perpendicular collagen, with its brush-like structure, can inhibit osteoblastic differentiation or expression of osteoblastic phenotype, thus preventing calcification. On the contrary, mesenchymal cells would readily differentiate into osteoblasts and form bone when encountering parallel collagen sheet. With this notion in mind, we like to take our hypothesis to the next level and predict that the establishment of perpendicular connective tissue attachment will lead the way to an innovative implant system with peri-implant ligament. We believe that a “periodontio-integrated” dental implant would potentially allow for a more dynamic role superior to the current osseointegrated implants. Since the periodontal Ruffini endings in the periodontal ligament are the major mechanoreceptors and are known for their neuroplasticity in response to stress and strain, we would like to conduct further studies to examine the feasibility of nerve regeneration around dental implants.

References

1. Branemark PI, Adell R, Albrektsson T, Lekholm U, Lundkvist S, Rockler B. Osseointegrated titanium fixtures in the treatment of edentulousness. Biomaterials 1983;4:25-28.

2. Albrektsson T, Branemark PI, Hansson HA, Lindstrom J. Osseointegrated titanium implants. Requirements for ensuring a long-lasting, direct bone-to-implant anchorage in man. Acta Orthop Scand 1981;52:155-170.

3. Schwarz F, Derks J, Monje A, Wang HL. Peri-implantitis. J Periodontol 2018;89 Suppl 1:S267-S290.

4. Derks J, Tomasi C. Peri-implant health and disease. A systematic review of current epidemiology. J Clin Periodontol 2015;42 Suppl 16:S158-171.

5. Esposito M, Thomsen P, Ericson LE, Sennerby L, Lekholm U. Histopathologic observations on late oral implant failures. Clin Implant Dent Relat Res 2000;2:18-32.

6. Lindhe J, Meyle J, Group DoEWoP. Peri-implant diseases: Consensus Report of the Sixth European Workshop on Periodontology. J Clin Periodontol 2008;35:282-285.

7. Hiyari S, Wong RL, Yaghsezian A, Naghibi A, Tetradis S, Camargo PM, et al. Ligature-induced peri-implantitis and periodontitis in mice. J Clin Periodontol 2018;45:89-99.

8. Giannobile WV. Getting to the root of dental implant tissue engineering. J Clin Periodontol 2010;37:747-749.

9. Nevins M, Nevins ML, Camelo M, Boyesen JL, Kim DM. Human histologic evidence of a connective tissue attachment to a dental implant. Int J Periodontics Restorative Dent 2008;28:111-121.

10. Gomez-Florit M, Xing R, Ramis JM, Taxt-Lamolle S, Haugen HJ, Lyngstadaas SP, et al. Human gingival fibroblasts function is stimulated on machined hydrided titanium zirconium dental implants. J Dent 2014;42:30-38.

11. Biggs MJ, Richards RG, Gadegaard N, McMurray RJ, Affrossman S, Wilkinson CD, et al. Interactions with nanoscale topography: adhesion quantification and signal transduction in cells of osteogenic and multipotent lineage. J Biomed Mater Res A 2009;91:195-208.

12. Robin A, Bernardes de Almeida Ribeiro M, Luiz Rosa J, Zenhei Nakazato R, Borges Silva M. Formation of TiO2 Nanotube Layer by Anodization of Titanium in Ethylene Glycol-H2O Electrolyte. Journal of Surface Engineered Materials and Advanced Technology 2014;04:123-130.

13. Kang C-G, Park Y-B, Choi H, Oh S, Lee K-W, Choi S-H, et al. Osseointegration of Implants Surface-Treated with Various Diameters of TiO2Nanotubes in Rabbit. Journal of Nanomaterials 2015;2015:1-11.

14. Carranza FA NM. Anatomy of the Periodontium. Carranza's Clinical Periodontology: Elsevier, 2015.

15. Zhu J, Kaufman LJ. Collagen I self-assembly: revealing the developing structures that generate turbidity. Biophys J 2014;106:1822-1831.

16. Shoulders MD, Raines RT. Collagen structure and stability. Annu Rev Biochem 2009;78:929-958.

17. Knight CG, Morton LF, Peachey AR, Tuckwell DS, Farndale RW, Barnes MJ. The collagen-binding A-domains of integrins alpha(1)beta(1) and alpha(2)beta(1) recognize the same specific amino acid sequence, GFOGER, in native (triple-helical) collagens. J Biol Chem 2000;275:35-40.

18. Brody AR. Control of lung fibroblast proliferation by macrophage-derived platelet-derived growth factor. Ann N Y Acad Sci 1994;725:193-199.

19. Habenicht AJ, Salbach P, Goerig M. Eicosanoid synthesis in platelet-derived growth factor-stimulated fibroblasts. Adv Exp Med Biol 1988;243:55-59.

20. Millette E, Rauch BH, Kenagy RD, Daum G, Clowes AW. Platelet-derived growth factor-BB transactivates the fibroblast growth factor receptor to induce proliferation in human smooth muscle cells. Trends Cardiovasc Med 2006;16:25-28.

21. Sculean A, Gruber R, Bosshardt DD. Soft tissue wound healing around teeth and dental implants. J Clin Periodontol 2014;41 Suppl 15:S6-22.

22. Thoma DS, Muhlemann S, Jung RE. Critical soft-tissue dimensions with dental implants and treatment concepts. Periodontol 2000 2014;66:106-118.

23. Bosshardt DD, Lang NP. The junctional epithelium: from health to disease. J Dent Res 2005;84:9-20.

24. Jiang Q, Yu Y, Ruan H, Luo Y, Guo X. Morphological and functional characteristics of human gingival junctional epithelium. BMC Oral Health 2014;14:30.

25. Iglhaut G, Schwarz F, Winter RR, Mihatovic I, Stimmelmayr M, Schliephake H. Epithelial attachment and downgrowth on dental implant abutments--a comprehensive review. J Esthet Restor Dent 2014;26:324-331.

26. Fujiseki M, Matsuzaka K, Yoshinari M, Shimono M, Inoue T. An experimental study on the features of peri-implant epithelium: immunohistochemical and electron-microscopic observations. Bull Tokyo Dent Coll 2003;44:185-199.

27. Ikeda H, Yamaza T, Yoshinari M, Ohsaki Y, Ayukawa Y, Kido MA, et al. Ultrastructural and immunoelectron microscopic studies of the peri-implant epithelium-implant (Ti-6Al-4V) interface of rat maxilla. J Periodontol 2000;71:961-973.

28. Larjava H, Koivisto L, Hakkinen L, Heino J. Epithelial integrins with special reference to oral epithelia. J Dent Res 2011;90:1367-1376.

29. Sugawara S, Maeno M, Lee C, Nagai S, Kim DM, Da Silva J, et al. Establishment of Epithelial Attachment on Titanium Surface Coated with Platelet Activating Peptide. PLoS One 2016;11:e0164693.

30. Maeno M, Lee C, Kim DM, Da Silva J, Nagai S, Sugawara S, et al. Function of Platelet-Induced Epithelial Attachment at Titanium Surfaces Inhibits Microbial Colonization. J Dent Res 2017:22034516688888.

31. Schroeder HE, Listgarten MA. The gingival tissues: the architecture of periodontal protection. Periodontol 2000 1997;13:91-120.

32. Berglundh T, Lindhe J, Ericsson I, Marinello CP, Liljenberg B, Thomsen P. The soft tissue barrier at implants and teeth. Clin Oral Implants Res 1991;2:81-90.

33. Nevins M, Kim DM, Jun SH, Guze K, Schupbach P, Nevins ML. Histologic evidence of a connective tissue attachment to laser microgrooved abutments: a canine study. Int J Periodontics Restorative Dent 2010;30:245-255.

34. Moon IS, Berglundh T, Abrahamsson I, Linder E, Lindhe J. The barrier between the keratinized mucosa and the dental implant. An experimental study in the dog. J Clin Periodontol 1999;26:658-663.

35. Buser D, Weber HP, Donath K, Fiorellini JP, Paquette DW, Williams RC. Soft tissue reactions to non-submerged unloaded titanium implants in beagle dogs. J Periodontol 1992;63:225-235.

36. Listgarten MA, Buser D, Steinemann SG, Donath K, Lang NP, Weber HP. Light and transmission electron microscopy of the intact interfaces between non-submerged titanium-coated epoxy resin implants and bone or gingiva. J Dent Res 1992;71:364-371.

37. Comut AA, Weber HP, Shortkroff S, Cui FZ, Spector M. Connective tissue orientation around dental implants in a canine model. Clin Oral Implants Res 2001;12:433-440.

38. Schwarz F, Herten M, Sager M, Wieland M, Dard M, Becker J. Histological and immunohistochemical analysis of initial and early subepithelial connective tissue attachment at chemically modified and conventional SLA titanium implants. A pilot study in dogs. Clin Oral Investig 2007;11:245-255.

39. Abrams GA, Goodman SL, Nealey PF, Franco M, Murphy CJ. Nanoscale topography of the basement membrane underlying the corneal epithelium of the rhesus macaque. Cell Tissue Res 2000;299:39-46.

40. Curtis A, Wilkinson C. Nantotechniques and approaches in biotechnology. Trends Biotechnol 2001;19:97-101.

41. Liu X, Chu PK, Ding C. Surface modification of titanium, titanium alloys, and related materials for biomedical applications. Materials Science and Engineering: R: Reports 2004;47:49-121.

42. Venkatachalam N, Palanichamy M, Murugesan V. Sol–gel preparation and characterization of nanosize TiO2: Its photocatalytic performance. Materials Chemistry and Physics 2007;104:454-459.

43. Tan AW, Pingguan-Murphy B, Ahmad R, Akbar SA. Review of titania nanotubes: Fabrication and cellular response. Ceramics International 2012;38:4421-4435.

44. Narayanan R, Kwon T-Y, Kim K-H. TiO2 nanotubes from stirred glycerol/NH4F electrolyte: Roughness, wetting behavior and adhesion for implant applications. Materials Chemistry and Physics 2009;117:460-464.

45. Awad NK, Edwards SL, Morsi YS. A review of TiO2 NTs on Ti metal: Electrochemical synthesis, functionalization and potential use as bone implants. Mater Sci Eng C Mater Biol Appl 2017;76:1401-1412.

46. Roy P, Berger S, Schmuki P. TiO2 nanotubes: synthesis and applications. Angew Chem Int Ed Engl 2011;50:2904-2939.

47. Diebold U. The surface science of titanium dioxide. Surface Science Reports 2003;48:53-229.

48. Brunette DM. Titanium in medicine : material science, surface science, engineering, biological responses, and medical applications. Berlin ; New York: Springer, 2001.

49. Chang S-W, Buehler MJ. Molecular biomechanics of collagen molecules. Materials Today 2014;17:70-76.

50. Egli J, Erdmann RS, Schmidt PJ, Wennemers H. Effect of N- and C-terminal functional groups on the stability of collagen triple helices. Chem Commun (Camb) 2017;53:11036-11039.

51. Civantos A, Martínez-Campos E, Ramos V, Elvira C, Gallardo A, Abarrategi A. Titanium Coatings and Surface Modifications: Toward Clinically Useful Bioactive Implants. ACS Biomaterials Science & Engineering 2017;3:1245-1261.

52. Seuss S, Boccaccini AR. Electrophoretic deposition of biological macromolecules, drugs, and cells. Biomacromolecules 2013;14:3355-3369.

53. Ling T, Lin J, Tu J, Liu S, Weng W, Cheng K, et al. Mineralized collagen coatings formed by electrochemical deposition. J Mater Sci Mater Med 2013;24:2709-2718.

54. Hohn S, Braem A, Neirinck B, Virtanen S. Albumin coatings by alternating current electrophoretic deposition for improving corrosion resistance and bioactivity of titanium implants. Mater Sci Eng C Mater Biol Appl 2017;73:798-807.

55. Blair P, Flaumenhaft R. Platelet alpha-granules: basic biology and clinical correlates. Blood Rev 2009;23:177-189.

56. Kaigler D, Avila G, Wisner-Lynch L, Nevins ML, Nevins M, Rasperini G, et al. Platelet-derived growth factor applications in periodontal and peri-implant bone regeneration. Expert Opin Biol Ther 2011;11:375-385.

57. Nevins M, Camelo M, Nevins ML, Schenk RK, Lynch SE. Periodontal regeneration in humans using recombinant human platelet-derived growth factor-BB (rhPDGF-BB) and allogenic bone. J Periodontol 2003;74:1282-1292.

58. Cavallo C, Roffi A, Grigolo B, Mariani E, Pratelli L, Merli G, et al. Platelet-Rich Plasma: The Choice of Activation Method Affects the Release of Bioactive Molecules. Biomed Res Int 2016;2016:6591717.

59. Fufa D, Shealy B, Jacobson M, Kevy S, Murray MM. Activation of platelet-rich plasma using soluble type I collagen. J Oral Maxillofac Surg 2008;66:684-690.

60. Mazzocca AD, McCarthy MB, Chowaniec DM, Cote MP, Romeo AA, Bradley JP, et al. Platelet-rich plasma differs according to preparation method and human variability. J Bone Joint Surg Am 2012;94:308-316.

61. Intini G, Andreana S, Intini FE, Buhite RJ, Bobek LA. Calcium sulfate and platelet-rich plasma make a novel osteoinductive biomaterial for bone regeneration. J Transl Med 2007;5:13.

62. Marx RE, Carlson ER, Eichstaedt RM, Schimmele SR, Strauss JE, Georgeff KR. Platelet-rich plasma: Growth factor enhancement for bone grafts. Oral Surg Oral Med Oral Pathol Oral Radiol Endod 1998;85:638-646.

63. Marx RE. Platelet-rich plasma: evidence to support its use. J Oral Maxillofac Surg 2004;62:489-496.

64. <1-s2.0-S0142961298001331-main.pdf>.

65. Lacoste E, Martineau I, Gagnon G. Platelet concentrates: effects of calcium and thrombin on endothelial cell proliferation and growth factor release. J Periodontol 2003;74:1498-1507.

66. Galli C, Passeri G, Cacchioli A, Gualini G, Ravanetti F, Elezi E, et al. Effect of laser-induced dentin modifications on periodontal fibroblasts and osteoblasts: a new in vitro model. J Periodontol 2009;80:1648-1654.

67. Nishimura K, Hayashi M, Matsuda K, Shigeyama Y, Yamasaki A, Yamaoka A. The chemoattractive potency of periodontal ligament, cementum and dentin for human gingival fibroblasts. J Periodontal Res 1989;24:146-148.

68. Renshaw MW, Price LS, Schwartz MA. Focal adhesion kinase mediates the integrin signaling requirement for growth factor activation of MAP kinase. J Cell Biol 1999;147:611-618.

69. Subramanian K, Tran D, Nguyen KT. Chapter 8 - Cellular responses to nanoscale surface modifications of titanium implants for dentistry and bone tissue engineering applications. In: Subramani K, Ahmed W (eds). Emerging Nanotechnologies in Dentistry (Second Edition): William Andrew Publishing, 2018:137-163.

70. Park J, Bauer S, Schlegel KA, Neukam FW, von der Mark K, Schmuki P. TiO2 nanotube surfaces: 15 nm--an optimal length scale of surface topography for cell adhesion and differentiation. Small 2009;5:666-671.

71. Smith BS, Yoriya S, Johnson T, Popat KC. Dermal fibroblast and epidermal keratinocyte functionality on titania nanotube arrays. Acta Biomater 2011;7:2686-2696.

72. Biela SA, Su Y, Spatz JP, Kemkemer R. Different sensitivity of human endothelial cells, smooth muscle cells and fibroblasts to topography in the nano-micro range. Acta Biomater 2009;5:2460-2466.

73. Goreham RV, Mierczynska A, Smith LE, Sedev R, Vasilev K. Small surface nanotopography encourages fibroblast and osteoblast cell adhesion. RSC Advances 2013;3:10309-10317.

74. Esfahanizadeh N, Motalebi S, Daneshparvar N, Akhoundi N, Bonakdar S. Morphology, proliferation, and gene expression of gingival fibroblasts on Laser-Lok, titanium, and zirconia surfaces. Lasers Med Sci 2016;31:863-873.

75. Takemoto S, Yamamoto T, Tsuru K, Hayakawa S, Osaka A, Takashima S. Platelet adhesion on titanium oxide gels: effect of surface oxidation. Biomaterials 2004;25:3485-3492.

76. Park JW, Han SH, Hanawa T. Effects of Surface Nanotopography and Calcium Chemistry of Titanium Bone Implants on Early Blood Platelet and Macrophage Cell Function. Biomed Res Int 2018;2018:1362958.

77. McDougall S, Dallon J, Sherratt J, Maini P. Fibroblast migration and collagen deposition during dermal wound healing: mathematical modelling and clinical implications. Philos Trans A Math Phys Eng Sci 2006;364:1385-1405.

78. Negmadjanov U, Holmuhamedov A, Emelyanova L, Xu H, Rizvi F, Ross GR, et al. TGF-β1 Increases Resistance of NIH/3T3 Fibroblasts Toward Apoptosis Through

Activation of Smad2/3 and Erk1/2 Pathways. Journal of Patient-Centered Research and Reviews 2016;3:187-198.

79. Galvis L, Dunlop JW, Duda G, Fratzl P, Masic A. Polarized Raman anisotropic response of collagen in tendon: towards 3D orientation mapping of collagen in tissues. PLoS One 2013;8:e63518.

80. Masic A, Bertinetti L, Schuetz R, Galvis L, Timofeeva N, Dunlop JW, et al. Observations of multiscale, stress-induced changes of collagen orientation in tendon by polarized Raman spectroscopy. Biomacromolecules 2011;12:3989-3996.

81. Schrof S, Varga P, Galvis L, Raum K, Masic A. 3D Raman mapping of the collagen fibril orientation in human osteonal lamellae. J Struct Biol 2014;187:266-275.

82. Bergholt MS, St-Pierre JP, Offeddu GS, Parmar PA, Albro MB, Puetzer JL, et al. Raman Spectroscopy Reveals New Insights into the Zonal Organization of Native and Tissue-Engineered Articular Cartilage. ACS Cent Sci 2016;2:885-895.

83. Chai WL, Moharamzadeh K, Brook IM, Emanuelsson L, Palmquist A, van Noort R. Development of a novel model for the investigation of implant-soft tissue interface. J Periodontol 2010;81:1187-1195.

84. Bates C, Marino V, Fazzalari NL, Bartold PM. Soft tissue attachment to titanium implants coated with growth factors. Clin Implant Dent Relat Res 2013;15:53-63.

85. Berglundh T, Lindhe J, Jonsson K, Ericsson I. The topography of the vascular systems in the periodontal and peri-implant tissues in the dog. J Clin Periodontol 1994;21:189-193.

86. Nishimoto SK, Nishimoto M, Park SW, Lee KM, Kim HS, Koh JT, et al. The effect of titanium surface roughening on protein absorption, cell attachment, and cell spreading. Int J Oral Maxillofac Implants 2008;23:675-680.

87. Kusakawa Y, Yoshida E, Hayakawa T. Protein Adsorption to Titanium and Zirconia Using a Quartz Crystal Microbalance Method. BioMed Research International 2017;2017:8.

88. Matcher SJ. What can biophotonics tell us about the 3D microstructure of articular cartilage? Quant Imaging Med Surg 2015;5:143-158.

89. Cox G, Kable E. Second-harmonic imaging of collagen. Methods Mol Biol 2006;319:15-35.

90. Kazanci M, Wagner HD, Manjubala NI, Gupta HS, Paschalis E, Roschger P, et al. Raman imaging of two orthogonal planes within cortical bone. Bone 2007;41:456-461.

91. Masic A, Schuetz R, Bertinetti L, Li C, Siegel S, Metzger H, et al. Multiscale Analysis of Mineralized Collagen Combining X-ray Scattering and Fluorescence with Raman Spectroscopy under Controlled Mechanical, Thermal, and Humidity Environments. ACS Biomaterials Science & Engineering 2017;3:2853-2859.